Published in final edited form as:
ACS Nano. 2013 June 25; 7(6): 4855–4868. doi:10.1021/nn305872d.

Cellular Interaction and Toxicity Depends on Physiochemical Properties and Surface Modification of Redox Active Nanomaterials

Janet M. Dowding[‡,1], **Soumen Das**[‡,2], **Amit Kumar**[2], **Talib Dosani**[1], **Rameech McCormack**[2], **Ankur Gupta**[2], **Thi X. T. Sayle**[3], **Dean C. Sayle**[3], **Laurence von Kalm**[4], **Sudipta Seal**[*,2], and **William T. Self**[*,1]

[1]Burnett School of Biomedical Science, College of Medicine, University of Central Florida, Orlando, Florida

[2]Nanoscience Technology Center, University of Central Florida, Orlando, Florida

[3]School of Physical Sciences, University of Kent, Canterbury CT2 7NZ, United Kingdom

[4]Department of Biology, College of Science, University of Central Florida, Orlando, Florida

Abstract

The study of the chemical and biological properties of CeO_2 NPs (CNPs) has expanded recently due to its therapeutic potential, and the methods used to synthesize these materials are diverse. Moreover, conflicting reports exists regarding the toxicity of CNP. To help resolve these discrepancies, we must first determine whether CeO_2 NPs made by different methods are similar or different in their physiochemical and catalytic properties. In this paper, we have synthesized several forms of CNPs using identical precursors through a wet chemical process but using different oxidizer/reducer H_2O_2 (CNP1), NH_4OH (CNP2) or hexamethylenetetramine (HMT-CNP1). Physiochemical properties of these CeO_2 NPs were extensively studied and found to be different depending on the preparation methods. Unlike CNP1 and CNP2, HMT-CNP1 were

[*]Corresponding Authors, William.Self@ucf.edu, (407) 823-4262, 4000 Central Florida Blvd., Bldg. 20 Room 124, Orlando, FL 32816-2364. Sudipta.Seal@ucf.edu, 4000 Central Florida Blvd, Eng 1, Room 381, Orlando, FL 32816.
[‡]Authors contributed equally to this work
[1]**Present Addresses**. Burnett School of Biomedical Science, College of Medicine, University of Central Florida, Orlando, Florida
[2]Nanoscience Technology Center, University of Central Florida, Orlando, Florida

ASSOCIATED CONTENT

SEAD spectra (FigureS1); Hydrodynamic radius (Figure S2); Surface chemistry (Figure S3); FTIR Spectra of different CNP nanoparticles (Figure S4); DSC-TGA analysis (Figure S5); CLSM images of nanoparticles intracellular aggregation at higher concentration (Figure S7); Cell viability and ATP levels at higher concentrations (Figure S8); Co-localization images (Figure S9); Toxicity profile of CNP on Drosophila melanogaster (Figure S10); pNPP and ATP hydrolysis by various preparations of CeO2 (Figure S11); ATPase activity of CNP1 (Figure S12); ATPase activity of different CNP nanoparticles I nthe presence of FBS (Figure S13); Raman Spectra of different CNP nanoparticles (Figure S13); Catalytic activities of different CNP nanoparticles (Figure S14); Hydrodynamic radius in media (Table S1). This material is available free of charge *via* the Internet at http://pubs.acs.org.

Author Contributions

Janet M. Dowding‡-experimental and manuscript writing
Soumen Das‡- experimental and manuscript writing
Amit Kumar-experimental contribution
Talib Dosani- experimental contribution
Rameech McCormack-experimental contribution
Ankur Gupta- experimental contribution
Thi X. T. Sayle- experimental contribution
Dean C. Sayle- Senior Author
Laurence von Kalm- Senior Author
Sudipta Seal- Corresponding Author
William T. Self - Corresponding Author

readily taken into endothelial cells and their aggregation can be visualized using light microscopy. Exposure to HMT-CNP1 also reduced cell viability (MTT) at a 10-fold lower concentration than CNP1 or CNP2. Surprisingly, exposure to HMT-CNP1 led to substantial decreases in the ATP levels. Mechanistic studies revealed that HMT-CNP1 exhibited substantial ATPase (phosphatase) activity. Though CNP2 also exhibits ATPase activity, CNP1 lacked ATPase activity. The difference in catalytic (ATPase) activity of different CeO_2 NPs preparation may be due to differences in their morphology and oxygen extraction energy. These results suggest the combination of increased uptake and ATPase activity of HMT-CNP1 may underlie the biomechanism of the toxicity of this preparation of CNPs, and may suggest ATPase activity should be considered when synthesizing CNPs for use in biomedical applications.

Keywords

cerium oxide nanoparticles; phosphatase activity; toxicity; surface modification; nanoparticles-cell interaction

Cerium is a rare earth metal that belongs to the Lanthanides series of the periodic table and its derivatives are used in many industrial applications.[1] Cerium in its oxide form has a fluorite structure. However in the nanoscale regime, CeO_2 NPs (CNPs) retain their fluorite structure with oxygen deficiencies, yielding CeO_{2-x}, with vacancies as the most likely sites for reduction-oxidation (redox) reactions.[2] This unique property of CNPs make it useful for industrial applications including the removal of carbon monoxide (CO), hydrocarbons and nitric oxide species (NO_x) from exhaust gas.[3] This property of CNPs is facilitated by the ability of CNPs to mediate its oxidation state between 3+ and 4+. The redox potential of CNPs favors the cycling of cerium to scavenge a variety of reactive oxygen species (ROS) and reactive nitrogen species (RNS) species.[4–7] Moreover, at the same time the unique oxygen buffering capacity of CNP allows the regeneration of its trivalent oxidation state (for further scavenging of radicals) without entering into deleterious side reactions for regeneration. The unique regenerative ability to scavenge ROS/RNS species has led to CNPs testing as potential therapeutics in numerous biological systems to reduce potentially harmful ROS/RNS in disease and aging. These studies include the protection of biological tissues against radiation induced damage,[8] prevention against laser induced retinal damage,[9] induction of angiogenesis through modulation of oxygen,[10] reduction of spinal injury,[11] reduction of chronic inflammation[12] and control or reduction of the growth and proliferation of tumors and inhibition of the tumorstroma interactions.[12, 13]

Nanoparticles in general exhibit novel surface properties and chemistry that influence their interaction with biological systems. For CNPs to be a realistic therapeutic, they must undergo a careful materials and biological characterization in order to insure safety. Part of that understanding must include a variety of synthesis processes in which the CNPs have been created. The methods used inpreparation of CNPs are widely varied;[14] this includes creating NPs with the core CeO_2 nanomaterial with different size, shape, surface modification and stability of the nanoparticles modifications.[14,15] Even when synthesizing ‘bare’ CNPs, there are numerous synthesis methods that have been employed.[14, 16–18] Over the past decades, synthesis methods for CNPs use have been extensively tested for industrial[19] and biological uses.[20] These methods include hydrolysis, precipitation, thermal deposition, combustion or flame-synthesis, sol-gel, hydrothermal or solvothermal, microemulsion method, gas condensation, sonochemical synthesis, and electrochemical synthesis among others.[14] Several preparation processes and surface coatings have been reported for CNPs for increasing bio-compatibility, decreased nonspecific interaction and stabilization in biological media.[21] Catalytic properties of room temperature/wet chemical synthesis of CeO_2 NPs have been well studied.[4–7] The rationale for this synthesis method is

that they seem to be less toxic[22–24] and the ability to control the Ce^{3+}/Ce^{4+} ratio.[25] On the other hand, hexamethylenetetramine (HMT) based synthesis of CNPs is also routinely employed and several reports exist on toxicological properties of this preparation both *in vitro* and *in vivo*. However, physiochemical and catalytic properties of hexamethylenetetramine (HMT) based synthesis of CeO_2 NPs[26–29] were not studied as extensively. Indeed, for CNPs to be a potential therapy for the reduction of ROS/RNS in disease, the mechanism of action for CNPs, respective of synthesis procedure, must be well defined. Unfortunately, the material synthesis of these studies varies significantly. Thus it must first be determined whether CNPs made by different methods are similar or different in their physiochemical properties. Therefore the next step is to determine the pathways that CNPs might antagonize or augment based on their synthesis. The underlying mechanisms of anti-oxidant or pro-oxidant properties of CNPs are now being determined by several groups. However, the outcomes of CNP exposure can vary as much as the synthesis methods and cell types tested.[30–32] This underscores the need to fully understand the nanoparticles physiochemical properties from different synthesis methods, possibly resulting in different catalytic behavior(s) and their influence(s) in various biological settings (from toxicity to therapeutics). Compared to other non-redox active nanoparticles, synthesis procedures of CNP (redox active) need to be well controlled to ensure consistency since catalytic/chemical properties of CNP from varying synthesis procedures may result in catalytically inactive or pro oxidant CNPs due to potential changes in the surface chemistry of the CNPs. Other than the CNPs antioxidant property, CNPs also exhibit phosphatase-like activity,[33] yet this activity is poorly understood and its biological relevance is not well understood.

Phosphorylation and dephosphorylation play a significant role in a wide range of important regulatory mechanisms in mammals. Control of the addition or removal of phosphate (PO_4^{3-}) groups is especially important for energy maintenance, and is particularly critical for adenosine triphosphate (ATP) which is a critical energy storage molecule. The hydrolysis of ATP to adenosine diphosphate (ADP) releases energy (H+) and inorganic phosphate which is then utilized in a wide range of cellular applications such as the movement of organelles (endosomes, lysosomes, mitochondria) along microtubules as well as muscle contractions, small molecule transport, or biosynthetic reactions driving anabolism. Any perturbation of ATP levels can have a significant effect on cellular physiology and metabolism, yet the ability of redox-active nanomaterials to alter ATP levels has rarely been carried out in previous studies.

In this study we compared CNPs synthesized using wet chemical methods varying the oxidizer/reductant (H_2O_2, NH_4OH precipitation, and HMT-based) to begin to understand the enigma of how CNPs can be reported to be both toxic and non-toxic when exposed to a variety of organisms and cells in culture at similar concentrations. Based on our results, the toxicity of HMT-CNPs may be due to differential cellular uptake and dissimilar catalytic properties of CNPs that proceeds through a poorly understood catalytic mechanism at the surface of the nanoparticle.

Results and Discussion

CNPs vary in size, shape, surface charge and physicochemical properties depending upon synthesis method

Careful characterization of nanoparticle preparations used in a study is critical when addressing catalytic properties and biological relevance. In this study we chose different synthesis procedures for making CNP and varying the physiochemical properties. These methods have been frequently used in the literature since it has been established that biological properties vary depending upon the synthesis method.[15] CNPs prepared using H_2O_2 (CNP1), NH_4OH (CNP2) or hexamethylenetetramine (HMT) (HMT-CNP1)were

characterized thoroughly. We modified the HMT preparation method to produce nanoparticles with varying amounts of HMT on the surface and to generate a spherical morphology. HMT-CNP2 (higher levels of HMT) was produced by omitting the acetone wash during the final washing stages. A spherical morphology of cerium oxide nanoparticles (HMT-CNP3) was produced by preheating the precursor solution. High resolution - transmission electron microscopy (HRTEM) images of all the nanoparticles are shown in Figure 1 ((a)-CNP1; (b)-CNP2, (c)-HMT-CNP1, (d)-HMT-CNP2 and (e)-HMT-CNP3)). Selected areas diffraction pattern (SEAD) confirmed the crystalline property of all the nanoparticles (Supplementary Figure S1). In general, CNP1 & CNP2 are smaller and rounder than the HMT-CNPs which display a sharp, angular shape. This demonstrates that depending upon synthesis method and the differing conditions during synthesis (see Materials and Methods) nanoparticles of the same cerium oxide composition (CeO_2) can be very different morphologically yet the biological relevance of these differences is poorly understood.

CNPs in general exhibit novel surface properties and change in nanoparticle morphology and surface properties due to different synthesis conditions, media and process can affect their interaction with biological systems. Table 1 contains a chart outlining the physico-chemical characteristics of all CNPs used throughout this study. The details of the synthesis are described in the methods section. Distribution of the hydrodynamic radius of individual particles is shown in Supplementary Figure S2a–e. Surface charge differences of CNPs (CNP1 and CNP2) and HMT CNPs were also estimated in dH_2O suspension. Additionally, Supplementary Table S1 contains data of the size and zeta potential of the various CNPs when in culture media for 4 or 24 hours. CNP's dispersed in culture media showed a slight increase in size as compared to water and zeta potential values changed from positive to slightly negative. The surface oxidation state (Ce^{3+}/Ce^{4+} ratio) of the CNPs preparations were calculated from x-ray photoelectron spectroscopy (XPS) data as described previously.[34] The intensity of peaks at 880.8, 885.8, 899.3 and 903.5 eV corresponding to the cerium (III) oxidation state and intensity of peaks at 881.9, 888.4, 897.9, 901.2, 906.8 and 916.3 eV corresponding to the cerium (IV) were determined and ratios calculated. Deconvoluted XPS spectra for all nanoparticles used in this study are shown in Supplementary Figure S3a–e. Fourier transform infrared spectroscopy (FTIR) spectra of hexamethyltetramine (HMT) and HMT-CNP1 revealed residual HMT on the surface of the HMT-CNP1 as compared with CNP1 (Supplementary Figure S4). The level of the organic was determined to contain HMT and was estimated by calculating differential scanning calorimetry - thermogravimetric analysis (DSC-TGA) by the percentage of weight loss.[35] TGA plots of thermal decomposition of HMT present on the surface of the HMT-CNPs is shown in Supplementary Figure S5a–c which confirmed the amount of HMT/organic contaminate on the surface of the nanoparticles. Moreover, XPS spectra of Nitrogen 1s (N 1s) of HMT-CNP1 also confirms presence of HMT on the surface of the nanoparticles. Interestingly, a shift in peak position of N 1s was observed for HMT-CNP1 (399.05 eV) compared to pure HMT (399.15 eV) (Supplementary Figure S6). The shift in peak position may be due to an interaction of HMT nitrogen with surface of the CNP1.

CNP1 and CNP2 were crystalline and due to their nanometer length scale, oxygen defects at the surface are present that yield reactive sites.[1] Within these sites, CNPs have the ability to interchange between the 3^+ and 4^+ oxidation states.[5] Two different CNPs exhibiting mixed Ce^{3+}/Ce^{4+}valence states were synthesized.[25] CNPs with a higher $3^+/4^+$ ratio of approximately 1.28 (CNP1) exhibits efficient superoxide dismutase (SOD) activity[5, 6] when compared to CeO_2 NPs with lower $3^+/4^+$ ratio of approximately 0.37 (CNP2). It should be noted that CeO_2 NPs with a lower $3^+/4^+$ ratio (CNP2) exhibit increased catalase mimetic activity[7] as well as the ability to effectively scavenge soluble nitric oxide (·NO).[4] HMT-based CNPs (HMT-CNP1, HMT-CNP2 or HMT-CNP3) contained lower $3^+/4^+$ ratios

measuring 0.37, 0.36, 0.32 respectively, very similar to CNP2, however without having any catalytic natures towards superoxide, hydrogen peroxide or ·NO (Supplementary Figure S15 a–e). HMT-CNP1 and HMT-CNP3 as synthesized contained very similar concentrations of HMT, 1.68 % and 1.78 % HMT respectively, however they differ in their shape with HMT-CNP1 morphology as polygonal and HMT-CNP3 morphology as round (Figure 1). HMT-CNP1 (1.68%) differed from HMT-CNP2 (8.16%) in the amount of HMT present on the surface of the nanoparticles. In addition, the mean hydrodynamic ratios of all three HMT-CNP's were increased when compared to CNP1 or CNP2.

Nanoparticles have high surface area to volume ratios and the physical properties of a nanoparticle can be dominated by the nature of the nanoparticle surface.[36] Particle size and surface area are important features when considering *in vivo* nano-bio reactivity.[37] High surface areas can also increase surface reactivity leading to catalytic activities that can be both beneficial and detrimental to cells.[15] The surface areas, as determined by BET, closely ranged between 71 and 118 m^2/g and it appeared that the presence of HMT had no dramatic influence on surface area.

HMT-based nanoparticles are more toxic than CNP1 or CNP2

The rapid development of CNPs for various potential applications in the field of nanomedicine has led to numerous studies evaluating CNP toxicity or biocompatibility. We employed the primary cell type Human Umbilical Vein Endothelial Cells (HUVECs) as a biological model to test toxicity in the context of human tissue. To investigate whether different particles made using different synthesis methods can effect overt toxicity, HUVEC cells were exposed to increasing CNP concentrations (0, 0.02, 0.08, 0.86, 8.6, 17 μg/mL) for 48 h (Figure 2). It should be noted that the HMT-CNPs were extensively washed during synthesis to avoid adsorption of background molecules of HMT onto the NPs so to prevent the residual HMT from affecting the NPs surface chemistry or be present in the aqueous portion of the samples (See Materials & Methods). We observed a reduced toxicity for CNP1, as previously reported[11] (Figure 2a) with similar observations for CNP2 (Figure 2b). Even at the highest concentrations (17 μg/mL), CNP1 and CNP2 only had modest effects on cell viability (20 %) whereas HMT-CNP1 showed a greater reduction in cell viability (30 %). However, at a ten-fold lower concentration (0.86 μg/mL) the HMT-CNP1 begin to exhibit a derogatory effect whereas the water-based, CNP1 and CNP2 did not (Figure 2c). To address whether the HMT concentration was responsible for the deceased cell viability, HMT-CNP2s which contain 8.16 % HMT (Figure 2d) were also tested and MTT results are similar to HMT-CNP1 (Figure 2c).

Sharp edges and corners present in the nanoparticles crystal structure may cause mechanical damage to the cell membrane which might also play a role in mediating toxicity to cells/living organism.[38] HMT-CNP1 have a polygonal shape and thus sharp edges. Therefore, to address if shape of the nanoparticle was a factor in toxicity, HMT-CNP3 containing similar concentration of HMT as HMT-CNP1 however having a rounder appearance (Figure 1e), similar to CNP1 and CNP2 (Figure 1a and 1b), were tested. MTT results for HMT-CNP3 (Figure 2e) were again similar to HMT-CNP1 strongly suggesting that increasing HMT concentration or shape did not play a role in the decreased HUVEC viability of HMT-CNP1 when compared to wet chemical based CNPs, CNP1 and CNP2. Additionally, all three HMT-CNPs started to show decreased cell viability at 0.86 μg/mL concentration whereas neither of the wet chemical based CNPs exhibit any toxicity at the 0.86 μg/mL concentration. To rule out that decreased cell viability was due solely to the presence of the HMT solvent, we tested the higher concentrations of HMT solvent only and found no toxicity to be attributed to the presence of the solvent alone (Figure 2f). The MTT assay relies upon metabolically active cells to reduce the MTT dye. The cell's source of energy is supplied by adenosine-5'-triphosphate (ATP) and is produced in mitochondria (*via* oxidative

phosphorylation) or by glycolysis (which take place in the cytoplasm). HUVECs are a primary cell line that primarily uses oxidative phosphorylation to acquire its energy. This led us to determine if intercellular ATP levels of HUVECs exposed to various preparations of CNPs were affected.

Exposure to HMT-CNP leads to decreases in intercellular ATP levels

To determine a possible mechanism linking exposure to HMT-CNPs and reduced HUVEC viability, we treated HUVECs with increasing CNP concentrations (0, 0.02, 0.08, 0.86, 8.6, 17 μg/mL) and measured ATP levels in cell lysates at 48 h as an alternative to MTT reduction. At the higher exposure concentrations (17 μg/mL), both CNP1 (Figure 3a) and CNP2 (Figure 3b) had diminished ATP levels (70-68%, respectively) as compared to controls. However, HMT-CNP1 treated cells showed dramatically reduced ATP levels at a twenty-fold lower exposure of 0.86 μg/mL (42 %) Figure 3c). We found similar decreases at the 0.86 μg/mL concentrations using HMT-CNP2 (Figure 3d) and HMT-CNP3 (Figure 3e). Similar to our MTT results, HMT solvent alone had no effect on ATP concentration (Figure 3f). Thus exposure to HMT-CNPs at lower doses resulted in a significant reduction in ATP levels than CNP1 or CNP2 exposure.

HMT-CNP1 aggregate in exposed HUVEC cells

CNPs are readily internalized by cells due to their small size. Since the HMT-CNPs all had similar toxicities (Figures 2 & 3) as well as phosphatase activities (to be discussed later in paper (Supplementary Figure S11c)) we chose to use HMT-CNP1 for additional in depth comparisons with CNP1 and CNP2. Untreated HUVECs as well as CNP1 and CNP2 (8.6 μg/mL) treated HUVECs exhibited no visible morphological changes (Figure 4a – c). Strikingly, HUVECs treated with HMT-CNP1 at the same concentration exhibited visible changes in morphology with live-cell imaging using 40× objective (Figure 4d). The ability to see nanoparticles using unaided microscopy techniques is uncommon. In the study by Yokel, *et. al.*, similar CeO_2 NP agglomerations were seen in light microscope images of spleen of rats treated with 250 mg/kg CeO_2 NPs after only 1 hour.[39] These intracellular accumulations led us to probe further the biological interaction of our CeO_2 NPs with HUVECs.

Confocal laser scanning microscopy (CLSM) images reveal perinuclear aggregation of HMT-CNP in HUVECs

It has been reported that CNPs dispersed directly into culture media may form aggregates after internalization into cells.[40] To confirm whether the dense granules visualized by bright field microscopy were actually HMT-CNP1 aggregates within the cell and not simply associated outside the cells, HUVECs were treated for 24 h with nanoparticles, washed repeatedly, trypsinized and seeded onto glass coverslips for 4 h (to allow for cell attachment) before fixation. Using immunocytochemistry we labeled the plasma membranes of HUVECs with wheat germ agglutinin (WGA) with fluorescein conjugate and took simultaneous fluorescent and bright field imaging using confocal microscopy. Untreated, CNP1 and CNP2 (8.6 μg/mL) treated HUVECs under bright field and merged channels show no evidence of nanoparticle aggregation (Figure 5a & b). By contrast, HUVECs treated with HMT-CNP1 (8.6 μg/mL) showed a robust increase in agglomerated, granular material in both the bright field and merged channels (Figure 5d). This aggregation becomes even more evident in HUVECs treated with a higher concentration of HMT-CNP1 (86 μg/mL) (Supplementary Figure S7) and at this concentration the nuclei are condensed indicating cells are dying or dead after only 24 h of treatment. Cell death is corroborated by MTT and ATP assays using the 86 μg/mL concentration (Supplemental Figure S8a & d). Notably, CLSM strongly suggested that the apparent dense granules were in fact intracellular HMT-CNP1s and their subcellular location was peri-nuclear. The subcellular localization is in agreement with

previous studies testing CNPs using *in vitro* cell culture models.[41] To explore the toxicity and drop in ATP concentrations by HMT-CNP1 further, we considered that the intercellular location of the HMT-CNP1 may play a role in their toxic nature. The wheat germ agglutinin (WGA) antibody used in Figure 5 and Supplementary Figure S7 specifically labels glycoproteins in plasma membranes as well the ER and Golgi – the location in the cells where sugars are incorporated into proteins in cells- in all cell images. We found the HMT-CNP1 aggregated in a peri-nuclear location aligning with the endoplasmic reticulum (ER) as visualized by WGA antibody. To further establish intercellular localization and in order to better visualize the HMT-CNP1, a fluorescent probe was conjugated to the HMT-CNP1 (FL-HMT-CNP1) and their subcellular localization determined with respect to mitochondria and lysosomes (Supplementary Figure S9). FL-HMT-CNP1 treated HUVEC cells were labeled with Mitotracker®. It did not appear that FL-HMT-CNP1 co-localize with mitochondria based on the merged image (Supplementary Figure S9b) suggesting the drop in ATP levels were not necessarily due to a direct interaction with mitochondria or proteins present in the electron transport chain including ATPases. Nanoparticles as well as most macromolecules are taken up in cells by the endosomal/lysosomal pathway. To determine if FL-HMT-CNP1 co-localized with lysosomes, HUVEC cells were labeled with Lysotracker® and a portion of the FL-HMT-CNP1 were found to co-localize with lysosomes (Supplementary Figure S9c). Together, these confocal studies demonstrate that the HMT-CNP1/FL-HMT-CNP1 appear to be located in the perinuclear region aligning with the ER and co-localizing mainly with lysosomes. Though the FL-HMT-CNP1 did not co-localize with mitochondria, mitochondria and ER are intimately connected and both play an essential role in cellular Ca^{2+} homeostasis.[42] It is possible a portion of the toxicity and drop in ATP concentrations is due to the aggregation of HMT-CNP1 and their cellular location, yet the decreases in ATP levels are likely due to the observed phosphatase activity given the localization of the particles.

HMT-CNP1 are transported into HUVECs more efficiently than water based cerium oxide nanoparticles

Uptake of nanomaterial varies vastly between materials tested and cell types.[43, 44] Based upon the morphological changes in HUVECs treated with HMT-CNP1 easily seen by light microscopy, we incubated HUVECs with increasing concentrations (0, 1.7, 8.6, 17, 86 μg/mL) of CNP1, CNP2 and HMT-CNP1 and harvested cells after 24 h. We used inductively coupled plasma mass spectrometry (ICP-MS) to determine the concentration of cerium inside the cells. Interestingly, CNP2 uptake was more efficient than CNP1 uptake and cellular uptake of HMT-CNP1 was greatly increased in HUVECs at every concentration tested (Figure 6). Detection of NPs at a concentration of 1.7 μg/mL by ICP-MS was nominal but our biological data (Figures 2 and 3) clearly demonstrates there is an effect in cell viability and ATP concentrations at 0.86 μg/mL for HMT-CNP1. This discrepancy may be due to the detectable limit of ICP-MS. When comparing the ATP levels, MTT assay data (Figures 2, 3 and Supplementary S8) and the uptake analysis, it is clear that at exposure to relatively low levels of HMT-CNP are impacting energy metabolism. If ATP hydrolysis is indeed occurring, the mitochondrial enzyme activity is possibly tryng to compensate in order to maintain sufficient ATP for cellular function. This likely explains why the MTT assay and ATP levels are not in complete agreement when assumed to reflect cell viability. Furthermore this is precisely why we followed the NPs using multiple methods in terms of subcellular localization (Figures 4, 5 and Supplementary S9). The zeta potentials of CNP1, CNP2 and HMT-CNP1 were very similar (~ −10) (Supplementary Table S1) therefore surface charge is not likely a major influence on the interaction of the particles with the cells. Thus the HMT contamination on the surface of the HMT-CNP1 might play an important role in increased cellular internalization as compared to CNP2 and CNP1. Taken together, this clearly shows that HMT-CNP1s are readily internalized by HUVEC cells and

this could be a contributing factor as to the toxicity previously observed in a *Caenorhabditis elegans* model[29] as well as their exhibiting an oxidant induced change in gene expression effect in a mouse neuronal model.[45] We tested CNP1 and HMT-CNP1 in a comparable model system, *Drosophila melanogaster* and found that CNP1 were not toxic and HMT-CNP1 NPs were only marginally toxic at a concentration of 86 μg/mL (Supplementary Figure S10) when fed to larvae. Though it is not practical to test the catalytic activity or size distribution in the Jazz® mix fly food, the nanoparticles were sonicated prior to addition to the food and particle size gradient distribution[46] allows for many sized particles and minimizes possible agglomeration effect of particles preventing uptake by the feeding larvae. However, these effects, if present, would be shared equally between all samples tested. Thus, uptake must be taken under consideration when determining toxicity as well as inherent differences in model systems, in our case *in vitro* cell culture toxicity vs whole animal marginal toxicity. Our ICP-MS data shows that the CNP2 are also readily taken up by HUVEC cells compared to CNP1, especially at higher concentrations, and yet they have not shown toxicity when compared to HMT-CNP1 in HUVECs. It should be noted that CNP2 exhibit catalase mimetic activity and scavenge ·NO[4, 7] and therefore these catalytic activities could be at the basis for their lack of toxicity.[47]

CNPs with increased surface 4+ character exhibit phosphatase and ATPase activity

Phosphorylation and dephosphorylation play significant roles in cell signaling, energy transfer and utilization within cells. Phosphate ester hydrolysis of biological molecules by CNPs would have important implications in their potential toxicity. In order to test any potential phosphatase activity of CNPs and HMT-CNPs, we first used *p*-nitrophenyl phosphate (pNPP) as a screening substrate.[33] This assay uses an artificial chromogenic substrate that is readily hydrolysed by phosphatases and allowed us to detect any potential phosphatase mimetic activity. We found that CNP2 as well as HMT-CNP1 were able to dephosphorylate pNPP whereas CNP1 did not (Supplementary Figure S11a). These results agreed with previous observations for ceria[33] and our initial results strongly suggested that CNPs with increased 4+ shared a similar catalytic activity. In order to corroborate the phosphatase mimetic activity and possibly explain the mechanism of cell death, we used ATP as the substrate and looked at free phosphate production using two different assays. Our results show again that CNP1 did not act as a phosphatase using ATP for the substrate (Supplementary Figure S12). SiO_2 NPs, a metal oxide NP of similar size was used as a negative control and also did not cause the release of phosphate (Supplementary Figure S11a–c). However, CNP2 and HMT-CNP1 did release phosphate from ATP with CNP2 showing a robust activity (Supplementary Figure 11b). To obtain quantitative information on the effect of CNP2 and HMT-CNP1, we determined the apparent K_m. Experimentally, we followed the kinetics of P_i released in a continuous reaction and determined the initial rates of free phosphate release from 34 μg/mL NPs in the presence of increasing concentrations of ATP (Figure 7a–d). The apparent K_m for HMT-CNP1 was 39.9 ± 8.2 μM. CNP2 were efficient phosphatases at lower substrate concentrations, however, when approaching physiological concentrations of ATP, CNP2s reached saturation and rates declined (Figure 7a). The CNP2 apparent K_m was determined to be 48.4 ± 10.6 μM. We compared the kinetic behavior of CeO_2 NPs with an established, physiologically relevant ATPase, dynein ATPase which has reported K_m of 20 μM.[48] We chose to compare to a motor protein since they have multiple active sites,[49] which is similar to nanoparticles having numerous oxygen vacancies for reactions to occur. In addition, dynein ATPase is located in the cytoplasm, along the same location as we saw the aggregation of HMT-CNP1 NPs (Figures 4 and 5). However, CNPs differ from dynein ATPase in terms of turnover rate. Dynein APTase V_{max} is 0.22 μM/s[48], however the V_{max} values for CNP1 and HMT-CNP1 were 0.017 nmol/min and 0.024 nmol/min (respectively).

Finally, to simulate the potential phosphatase activity of CNPs in cell culture, we measured pNPP hydrolysis in the presence of increasing amounts of fetal bovine serum (FBS). Nanoparticles in cells come into contact with various proteins and other molecules potentially forming a corona which is dynamic and is affected by particle material, size and surface properties.[50] In some cases the corona may lead to newly acquired nanoparticle properties.[37] Supplementary Figure S13 clearly demonstrates that CNP2 phosphatase activity diminishes with increasing concentrations of FBS whereas HMT-CNP1 phosphatase activity was not affected, even in the presence of up to 10 % FBS. Collectively, these results suggest that CNPs with increased level of 4+, regardless of their synthesis method, are competent phosphatases. They were able to hydrolyze various substrates including pNPP (Supplementary Figure S9a,c), ATP (Supplementary Figure S9b and Figure 8) and GTP (data not shown). Furthermore, shape (HMT-CNP2) and increased HMT concentration on the surface (HMT-NP3) were able to similarly hydrolyzed ATP when compared to HMT-CNP1 (Supplemental Figure S9c). However, HMT-CNP1 is more readily taken up by cells so the concentration of the catalyst is higher in cells than those exposed to CNP2. Additionally, the difference in phosphatase activity might be due to decreased surface area of the HMT-CNP1 (10–12 nm) as compared to CNP2 (3–5 nm) as well as HMT-CNP1's phosphatase activity is not affected by increasing concentrations of FBS. This suggests the protein-HMT nanoparticle corona appears to be less detrimental to their phosphatase activity as compared to the protein-CNP2 corona leading to a decreased level of CNP2 phosphatase activity. Presence of HMT molecules on the surface of the nanoparticles may also interfere with the interaction of ATP with CNP surface, which may also be one of the causes of decreased phosphatase activity of CNP-HMT-1 as compared to CNP2. Further to find out if oxygen vacancy on the surface of the nanoparticles may play a role in phosphatase activity, we estimated the oxygen vacancies using Raman Spectroscopy. Differences in surface oxygen vacancies of HMT-CNP1 and CNP2 were observed (Supplementary Figure S14). In particular both CNP2 and HMT CNP1 has similar Ce^{3+}/Ce^{4+} oxidation state ratios however oxygen vacancy of CNP2 was found to be $2.49 \pm 0.13 \times 10^{21}$ and $3.59 \pm 0.25 \times 10^{21}$ for HMT CNP2. Micro ceria were included as references, vacancy calculation showed less oxygen vacancy (1.16×10^{21}) as compared to nano sized particles. Therefore decreasing oxygen vacancies might also play a role in increasing the phosphatase activity of the nanoparticles. This can be explained by Scheme 1. Possible correlation of oxygen vacancy with catalytic property of the nanoparticles might be explained in terms of water dissociation and availability of −OH group on the surface of the nanoparticles. Oxygen vacancy strongly coordinates with -OH group and decreased the availability of −OH on the surface[51] which in turn decreases the phosphatase activity of the nanoparticles.

Synthesis method determines surface catalytic character of CNPs

Having identified ATPase as a critical catalytic character for HMT-CNPs in terms of toxicity, we tested these preparations of CNPs to assess the effect of synthesis on their catalytic activity at a broader level. To evaluate the potential catalytic activities we tested HMT-CNP1s for their ability to scavenge ·NO or to act as SOD or catalase mimetics. Unlike CNP1 or CNP2, HMT-CNP1s did not show any reactivity towards ·NO (Supplementary Figure S15a), superoxide (Supplementary Figure S15b), and hydrogen peroxide (Supplementary Figure S15c).

Reduction of Ce^{4+} to Ce^{3+} causes oxygen vacancies or defects on the surface of the crystalline lattice structure of the particles, generating a cage for redox reactions to occur.[52] It has been established that the specificity of some of the catalytic activities depend upon the ratio of Ce^{3+}/Ce^{4+}.[4, 53] Table 2 highlights how the wet chemical synthesis method of CNPs without HMT leads to unique physical and chemical/catalytic characteristics that are not found in CNPs synthesized by the HMT-based method. In addition, these catalytic activities

seem to correlate with the 3+/4+ ratio, specifically NPs with more Ce^{4+} displaying phosphatase activity. This reiterates the need for the careful characterization of nanoparticle preparations and a thorough understanding of their catalytic activities. These findings support previous publications showing toxicity of HMT-CNP based CeO2 NPs.[29, 45]

Correlation of nanoparticle morphology with reactivity

To help understand and interpret the different catalytic activities of CNP2 and CNP-HMT1 (both having similar Ce^{3+}/Ce^{4+} ratio), molecular dynamics (MD) simulation was used to generate full atomistic models of CNPs with different morphologies. The models were then used to interrogate their surface activity to enable a morphology-activity correlation. This information will help reveal whether the morphology of CNP can influence their chemical activity -specifically how the morphology might influence the ease of liberating oxygen from the surface of the nanoparticle.

Experimental fabrication of CNPs typically involves a crystallisation step during synthesis. Simulated amorphisation and crystallisation was used to generate full atomistic models for CNP's. The atomistic structures of two CNP's, with different morphologies, are shown in Figure 8. The first nanoparticle (Figure 8 a,b) exhibits a polyhedral morphology and exposes predominantly {111} surfaces together with a small amount of {100}. Conversely, the second CNP (Figure 8 c,d) appears more spherical and exposes at the surface a greater proportion of {100} compared to {111} surfaces. The nanoparticle with polyhedral morphology (Figure 8 a,b) is therefore a model representative of HMT-CNP1 and the pseudo-spherical nanoparticle (Figure 9 c,d) is a model representative of CNP2.

A comparison between the calculated activity 'fingerprints', Figure 8 b and d, for the polyhedral (HMT-CNP1) and spherical morphologies (CNP2) respectively, reveals the 'spherical' morphology/CNP2, Figure 8 d, is more active towards surface oxygen release compared to the CNP with polyhedral morphology/HMT-CNP1, Figure 8 b, which further supports our experimental, catalase and phosphatase activity observations of CNP2 and HMT CNP1. In particular, the {111} surfaces are predicted to be less active towards oxygen release from the surface compared to {100} surfaces. The simulations therefore predict that the morphology of CNP's can influence significantly their surface activity - specifically their ability to liberate oxygen from the surface.

Conclusion

The toxicology and surface reactivity of CeO_2 nanoparticles synthesized by two different methods were compared in this work in order to elucidate the mechanisms behind the varied observations with biological models in the current literature. In this study we showed that HMT-CNP1 are readily taken up by HUVECs and their aggregation was visible using conventional light microscopy techniques (Figures 5 and 6). An increase in the uptake of HMT-CNP1 certainly could have a negative effect on a HUVEC cell's metabolism along with their perinuclear aggregation. Compared to CNP2, enhanced cellular internalization of HMT-CNP1 may indicate residual surface HMT promotes cellular interaction and internalization of CNPs. However, the CNP2 are also taken up but do not aggregate (Figures 5 & 6), and the internalization is approximately one third as compared to HMT-CNP. The reduced, relative toxicity by CNP2 may be explained in terms of lower cellular internalization as compared to HMT CNP1 (Figure 7) as well as CNP2 are catalase mimetics [7] and scavenge soluble ·NO.[4]

Herein, we have demonstrated that synthesis methods of CNPs can further affect surface properties. For non-redox active nanoparticles, varying the synthesis procedure may not have a substantial effect but our data demonstrates that it is not the case when dealing with

redox active nanomaterials. A slight change in physico-chemical properties (Figure 2) can give you a vast difference in the redox properties of the nanomaterials (Table 2). Kuchma *et. al.* report that the phosphatase activity appears to be dependent upon the Cerium(III) sites.[33] It is possible that the ATPase activity seen in the CNP2 and HMT-CNP1 may be due to a nucleophile attraction of the Ce^{3+} and the terminal phosphate on an ATP molecule. Paradoxically, CNP1, which have more vacancies on the surface are not phosphatase mimetics. Moreover, simulation results reveled that morphology has also influence on nanoparticle reactivity, which may explain the lower phosphatase activity of HMT-CNP 1 as compared to CNP 2, while they have similar Ce^{3+}/Ce^{4+} ratios on the surface. Moreover, higher oxygen vacancy/decreased availability of -OH on the surface of HMT-CNP1 potentially make them less reactive towards phosphatase activity.

Although most of the focus of CeO_2 NP research has been on the ability of these materials to reduce reactive oxygen and nitrogen species in biological systems,[54] there are reports that claim that nanoceria are toxic. Unfortunately, the material synthesis methods used are not always clearly reported and it is likely that these observed toxicities are due to different physiochemical properties and unwanted surface modification. The CNPs synthesized in HMT resulted in different surface chemistry which resulted in different catalytic activities than the CNPs synthesized without HMT. The increased uptake and phosphatase/ATPase activity of HMT-CNP1 may underlie their toxicity. With the recent burgeoning growth of the use of CNPs as potential therapeutics, synthesis method and surface chemistries must be emphasized.

Materials and Methods

Preparation of different cerium oxide nanoparticles

In this study several CNPs were prepared with varying surface oxidation state, surface modification, and morphology. Cerium nitrate hexahydrate (99.999% pure from Sigma Aldrich, St. Louis, MO) was used as a precursor for all of the preparations. Cerium oxide nanoparticles with a higher Ce^{3+}/Ce^{4+} ratio (CNP1) or with lower Ce^{3+}/Ce^{4+} ratio (CNP 2) were prepared using wet chemical method as described previously.[55] Briefly, precursor dissolved in distilled water (dH_2O) and stoichiometric H_2O_2 (CNP1) or NH_4OH (CNP2) was added to the precursor solution. After addition of H_2O_2 (CNP1) or NH_4OH (CNP2) solutions were mixed properly. NH_4OH preparation was washed four times with ddH_2O and resuspended in same volume of water. pH of the both nanoparticles suspensions were then adjusted to 3 to get stable suspensions. Surface modified cerium oxide nanoparticles were prepared using hexamethylenetetramine (HMT).[56] Briefly, equal volumes of 37.5 mM cerium nitrate solution and 0.5 M HMT were mixed together and stirred for 24 h at room temperature. Cerium oxide nanoparticles prepared using HMT were washed with either ethanol and acetone or dH_2O for three times and finally resuspended in dH_2O. It is important to mention that after washing with ethanol and acetone, CNP-HMT1 was washed with dH_2O (three times) to remove any trace amount of solvent (ethanol or acetone) before resuspending in dH_2O. Cerium oxide nanoparticles washed with ethanol and acetone to remove the maximum amount of HMT were designated as CNP-HMT1. CNPs washed with only dH_2O were designated as HMT-CNP2. Different morphologies of CNP-HMT3 were prepared by preheating both the solutions (37.5 mM cerium nitrate precursor and 0.5 M HMT) at 60° C and then equal volumes of the solutions were mixed and stirred for 4 h. CNPs formed were then washed with ethanol and acetone for three times and finally with dH_2O to remove the solvent before resuspending in dH_2O. All the nanoparticles were aged for same amount of time (six weeks) before start the biological and catalytic experiment. Moreover, all the nanoparticles were stored at in room temperature and glass container to ensure similar storage condition and minimize any external influence. All the nanoparticles

used in different reactions were characterized thoroughly after six week of ageing and to ensure stable water dispersed nanoparticles.

Preparation of Fluorescence Conjugated HMT-CNP1

HMT ceria was partially coated with (3-amino) propyl trimethoxysilane. 1:0.1 molar ratio of HMT CeO_2:Silane was used for partial coating or amine functionalization and reaction were carried in Tolune. Excess silane was removed by washing. Then anime functionalized HMT CNP was conjugated to NHS-fluorescein using N-(3-dimethylaminopropyl)-N'-ethylcarbodiimide (EDC) and N-hydroxysuccinimide (NHS) chemistry.[57] Free fluorescence molecules were removed by washing with distilled water.

Physico-Chemical Properties of Cerium Oxide Nanoparticles (CeO_2)

High resolution transmission electron microscopy (HRTEM) was used to analyze size and morphology of the nanoparticles. Hydrodynamic radius and surface charge of the nanoparticles were estimated using Zetasizer (Nano-ZS from Malvern Instruments, Houston, TX). X-Ray photoelectron spectroscopy (5400 PHI ESCA) was used to determine the surface oxidation state of the nanoparticles. Mg-Ka X-radiation (1253.6 eV) and 350 W power was used during the data collection as previously described.[55] Fourier transform infrared (FTIR) spectra were collected to confirm the presence of any HMT molecule on the nanoparticle surface using a PerkinElmer Spectrum IR Spectrophotometer (Waltham, MA). The amount of HMT that remains on the surface of the nanoparticles was determined with differential scanning calorimetry and thermogravimetric analysis (DSC-TGA) using a TA Instruments SDT-Q600 (New Castle, DE), with open alumina pans under 100 mL/min air flow. Particle size analysis was also carried out by measuring the specific surface area (m^2/g) using the Brunauer, Emmett, and Teller (BET) method with a Quantachrome Nova 4200e surface area analyzer (Boynton Beach, FL).

Cultivation of HUVECs

Human Umbilical Vein Endothelial Cells (HUVECs) (Lonza Walkerville, Inc., Walkersville, MD) were maintained at 37° C in a humidified atmosphere containing 5 % CO_2 in endothelial basal medium (EBM) (Lonza Walkerville, Inc., Walkersville, MD) supplemented with 2 % fetal bovine serum (FBS). Only cells from passages 3–6 were used in experiments.

Cell viability MTT assay

HUVECs were cultured in 96-well plates and exposed to CNPs for 48 h followed by addition of thiazoyl blue tetrazolium bromide (MTT) (Amresco, Solon, OH) (1.2 mM) as previously described.[58] Cell viability was determined by dividing the absorbance of treated samples to untreated controls and reported as a percentage of control cells. Results were collected from at least three independent experiments and are expressed as mean ± standard deviation (s.d.). Statistical analysis of two populations was compared using two-tailed non-paired Student's *t* test.

Analysis of intracellular ATP levels

HUVECs were cultured in opaque-walled 96-well plates and treated with CNPs for 48 h. Plates were equilibrated to room temperature and cells were lysed according to manufacturer instructions. CellTiter-Glo® Reagent was added and plates were incubated for 10 min to stabilize the luminescent signal. Luminescence was then recorded with a Varian Cary Eclipse fluorescence spectrophotometer (Palo Alto, CA) using 1 second integration time per well. Results were collected from at least three or more independent experiments and are

expressed as mean ± standard deviation (s.d.). Statistical analysis of two populations was compared using two-tailed non-paired Student's *t* test.

ICP-MS uptake of CNPs studies

HUVEC culture monolayers were incubated for 24 h with nanoparticles. Cells were washed two-times to remove extracellular nanoparticles and then collected by typsination and washed with PBS again to remove excess media and particles that could be adsorbed on the surface of the cells. Cells exposed to CNPs were analyzed for their cerium content using a Thermo Electron X-Series inductively coupled plasma mass spectrometer (ICP-MS, Thermo Scientific, Pittsburgh, PA) following APHA method 3125B to determine the amount of CNPs taken up by the cells.

Live cell imaging of HUVECs exposed to CNPs

HUVECs were cultured on Lab-Tek®II chambered coverglass (NUNC, Rochester, NY) slides in phenol red-free EBM (Lonza, Walkersville, MD) supplemented with 2 % FBS. Cells were exposed to various preparations of CeO_2 NPs for 36 h. To visualize nuclei, Hoechst 33342 dye (Molecular Probes, Invitrogen, Eugene, OR) (1μg/mL) was added to the medium for 10 min at 37° C in a humidified 5 % CO_2 incubator. Dye was removed and replaced with pre-warmed medium. Chamber slides with cultured HUVECs were examined under phase-contrast 40× air objective on a Nikon Eclipse Ti fluorescence microscope (Model # 602542, Melville, NY USA) and images acquired at 37° C in a humidified 5 % CO_2 atmosphere.

Confocal microscopy

HUVECs were exposed to nanoparticles for 24 h and subsequently washed, trypsinized and seeded onto glass coverslips for 4 h (to allow for cell attachment). Cells were then fixed in 4 % formaldehyde for 20 min at RT. Cells were washed two times in PBS and then labeled with wheat germ agglutinin (WGA), Alexa Fluor® 488 (Molecular Probes, Invitrogen, Eugene, OR) (5 μg/mL) for identification of plasma membranes (green channel, excitation 405nm/emission 498) and Hoechst 33342 for identification of nuclei (blue channel, excitation 405/emission 428). Cells were washed and mounted in anti-fade mounting media (Calbiochem, St. Louis, MO) and slides cured 24h at RT. Slides were stored at 4° C until simultaneous confocal and bright field imaging by Leica TCS SP5 laser scanning confocal microscope (Buffalo Grove, IL) with 40×/1.25 oil objective lens.

Phosphatase mimetic assay

To measure the phosphatase activity of various CNPs, 1.2 mM of *p*-nitrophenyl phosphate (pNPP) (New England BioLabs Inc., Ipswich, MA) was incubated in a 96-well plate in the presence of various concentrations of CNPs (4.3, 8.6, 17, 34 μg/mL) in a total volume of 200 μL H_2O. The ability of CNPs to catalyze the hydrolysis of pNPP to *p*-nitrophenyl was measured by following the increasing absorbance (405 nm) every minute for 20 min using a Spectramax 190 UV-visible spectrophotometer (Molecular Devices, Sunnyvale, CA).

ATPase activity assays

The concentration of inorganic phosphate liberated by various preparations of CNPs was determined using a malachite green assay (R&D Systems, Minneapolis, MN). Nanoparticles (34 μg/mL) were added to ATP or GTP (Sigma Aldrich St. Louis, MO) (34 μg/mL) at various time points (0, 30 sec, 1 min, 2 min, 4 min, 6 min, 8 min ,10 min) at room temperature in 50 mM Tris buffer at pH 8.0. A phosphate standard curve was generated to enable quantitative determination of phosphate. The Malachite Green solutions were added to each well and the absorbance (620 nm) was determined using a Spectramax 190 UV-

visible spectrophotometer (Molecular Devices, Sunnyvale, CA) after a 20 min incubation to stabilize the dye/PO_4 complex.

The concentration of inorganic phosphate liberated by various preparations of CNPs was also determined using the EnzCheck Phosphate Assay (Invitrogen, Grand Island, NY USA). The EnzCheck phosphate reaction is a fast, quantitative enzymatically linked assay in which in the presence of P_i the substrate 2-amino-6-mercapto-7-methylpurine riboside (MESG) is converted enzymatically by purine nucleoside phosphorylase (PNP) to ribose 1-phosphate and 2-amino-6-mercapto-7-methyl purine. The conversion of MESG can be followed by the increase in absorbance at 360 nm. Nanoparticles (34 μg/mL) were added to varying concentrations of ATP (Sigma Aldrich St. Louis, MO) and phosphate release followed every 30 sec for 30 min at 360 nm using a Spectramax 190 UV-visible spectrophotometer (Molecular Devices, Sunnyvale, CA) after initial 10 min incubation. A phosphate standard curve was generated to enable quantitative determination of phosphate in solution. Baseline changes due to hydrolysis of phosphate from ATP only controls was subtracted from each concentration to determine free phosphate liberated only by addition of CNPs. The kinetic parameters, V_{max} and K_m were calculated by using SigmaPlot® 10 software (Systat Software, Inc., Point Richmond, CA).

Drosophila melanogaster exposure to CNP1, CNP2 or HMT-CNP1 cerium oxide nanoparticles

Male and female wild-type *D. melanogaster* (Oregon R) were maintained under optimal conditions in a standard corn meal medium at a temperature of 25° C.[59] Exposure to nanoparticles began at the larval stage and continued through eclosion of adults. Parental crosses were set up in cages with 150 females and 30–40 males on grape plates seeded with live yeast. After 21 hours, each grape plate was changed and hatched larvae removed. Groups of 50 larvae from grape plates were isolated using a mounting needle under a dissecting microscope and placed in vials containing 6 ml Jazzmix (Fisher Scientific, Pittsburg, PA) food medium containing 86 μg/mL of nanoparticles, CNP1 or HMT-CNP1. Control larvae were cultured in parallel in food vials containing only H_2O or 500 μM HMT. All vials were kept at 25° C and checked daily for pupariation and eclosion. Statistical analysis was performed using one-way ANOVA followed by post hoc Tukey's test using Statistical Packages for the Social Sciences (SPSS) software.

Raman spectroscopy

Raman spectra were collected using a Horiba JobinYvon LabRam infrared (IR) micro-Raman system using a 633 nm helium-neon laser with a spatial resolution of 2 μm to obtain the electronic structure. Defect concentration of the nanomaterials were calculated using the following equations as described.[60, 61]

$$\Gamma(\mathrm{cm}^{-1}) = 5 + 5.81/\mathrm{d_g} \quad (1)$$

Where, Γ and d_g are half width at half maxima (HWHM) and grain size, respectively

$$L(nm) = \sqrt[3]{\left(\frac{\alpha}{2d_g}\right)^2}\left[(d_g - 2\alpha)^3 + 4{d_g}^2\alpha\right] \quad (2)$$

L is correlation length (average distance between two lattice defects) and α radius of CeO2 units (0.34 nm).

$$N = {}^{3}/_{4\pi L^{3}} \quad (3)$$

N is defect concentration.

Simulation

Simulated amorphisation and crystallisation was used to generate full atomistic models for CNP's. This method has been described in detail previously[62] and therefore only the salient details are presented below.

CNP's were cut from the parent bulk material and amorphised/melted by heating under MD simulation to temperatures above the melting point. Once molten, MD simulation was continued at temperatures below the melting point, which enabled crystalline seeds to spontaneously evolve and nucleate the crystallisation of the nanoparticle. A structural distribution of model nanoparticles was generated by altering the temperature of the crystallisation step. In particular, temperature changes led to differences in morphology and microstructure (such as dislocations, grain-boundaries).

Equipped with atomistic models, the surface activities of the CNP's were interrogated by determining the ease of extracting oxygen from the surface of the nanoparticle. We have shown previously that the energy required to extract oxygen from the surface of a CNP correlates with the electrostatic potential of the individual oxygen atoms comprising the nanoparticle[63] enabling visual 'activity fingerprints' to be generated. Accordingly, the activity fingerprints were calculated for the CNP's and presented graphically.

Supplementary Material

Refer to Web version on PubMed Central for supplementary material.

Acknowledgments

We thank Hoon Park and Dr. Alfons Schulte from UCF Department of Physics for their assistance with Raman spectroscopy. We thank Jeffery Hatcher and Dr. Jack Cheng from UCF Burnett School of Biomedical Science, Department of Medicine for assistance with confocal microscopy.

Funding Sources

This work is supported by NIH grant R01AG031529-01 as well as NSF grant NIRT CBET 0708172. Additional support includes CBET 1028996 (NSF International Supplement) and CBET 0804733 (NSF REU supplement to R. McCormick).

REFERENCES

1. Campbell CT, Peden CH. Chemistry. Oxygen Vacancies and Catalysis on Ceria Surfaces. Science. 2005; 309:713–714. [PubMed: 16051777]
2. Tsai YY, Oca-Cossio J, Lin SM, Woan K, Yu PC, Sigmund W. Reactive Oxygen Species Scavenging Properties of ZrO2-CeO2 Solid Solution Nanoparticles. Nanomedicine. 2008; 3:637–645. [PubMed: 18817467]
3. Masui T, Ozaki T, Machida K, Adachi G. Preparation of Ceria-Zirconia Sub-Catalysts for Automotive Exhaust Cleaning. J Alloy Compd. 2000; 303:49–55.
4. Dowding JM, Dosani T, Kumar A, Seal S, Self WT. Cerium Oxide Nanoparticles Scavenge Nitric Oxide Radical (·NO). Chem Commun. 2012; 48:4896–4898.
5. Heckert EG, Karakoti AS, Seal S, Self WT. The Role of Cerium Redox State in the SOD Mimetic Activity of Nanoceria. Biomaterials. 2008; 29:2705–2709. [PubMed: 18395249]

6. Korsvik C, Patil S, Seal S, Self WT. Superoxide Dismutase Mimetic Properties Exhibited by Vacancy Engineered Ceria Nanoparticles. Chem Commun. 2007; 0:1056–1058.
7. Pirmohamed T, Dowding JM, Singh S, Wasserman B, Heckert E, Karakoti AS, King JE, Seal S, Self WT. Nanoceria Exhibit Redox State-Dependent Catalase Mimetic Activity. Chem Commun. 2010; 46:2736–2738.
8. Tarnuzzer RW, Colon J, Patil S, Seal S. Vacancy Engineered Ceria Nanostructures for Protection From Radiation-Induced Cellular Damage. Nano Letters. 2005; 5:2573–2577. [PubMed: 16351218]
9. Chen J, Patil S, Seal S, McGinnis JF. Rare Earth Nanoparticles Prevent Retinal Degeneration Induced by Intracellular Peroxides. Nat Nano. 2006; 1:142–150.
10. Das S, Singh S, Dowding JM, Oommen S, Kumar A, Sayle TX, Saraf S, Patra CR, Vlahakis NE, Sayle DC, et al. The Induction of Angiogenesis by Cerium Oxide Nanoparticles Through the Modulation of Oxygen in Intracellular Environments. Biomaterials. 2012; 33:7746–7755. [PubMed: 22858004]
11. Das M, Patil S, Bhargava N, Kang JF, Riedel LM, Seal S, Hickman JJ. Auto-catalytic Ceria Nanoparticles Offer Neuroprotection to Adult Rat Spinal Cord Neurons. Biomaterials. 2007; 28:1918–1925. [PubMed: 17222903]
12. Hirst SM, Karakoti AS, Tyler RD, Sriranganathan N, Seal S, Reilly CM. Anti-inflammatory Properties of Cerium Oxide Nanoparticles. Small. 2009; 5:2848–2856. [PubMed: 19802857]
13. Alili L, Sack M, Karakoti AS, Teuber S, Puschmann K, Hirst SM, Reilly CM, Zanger K, Stahl W, Das S, et al. Combined Cytotoxic and Anti-Invasive Properties of Redox-Active Nanoparticles in Tumor-Stroma Interactions. Biomaterials. 2011; 32:2918–2929. [PubMed: 21269688]
14. Sun CW, Li H, Chen LQ. Nanostructured Ceria-Based Materials: Synthesis, Properties, and Applications. Energ Environ Sci. 2012; 5:8475–8505.
15. Karakoti AS, Munusamy P, Hostetler K, Kodali V, Kuchibhatla S, Orr G, Pounds JG, Teeguarden JG, Thrall BD, Baer DR. Preparation and Characterization Challenges to Understanding Environmental and Biological Impacts of Ceria Nanoparticles. Surf Interface Anal. 2012; 44:882–889. [PubMed: 23430137]
16. Bumajdad A, Eastoe J, Mathew A. Cerium Oxide Nanoparticles Prepared in Self-Assembled Systems. Adv Colloid Interface Sci. 2009; 147–148:56–66.
17. Karakoti AS, Kuchibhatla SVNT, Babu KS, Seal S. Direct Synthesis of Nanoceria in Aqueous Polyhydroxyl Solutions. J Phys Chem C. 2007; 111:17232–17240.
18. Sathyamurthy S, Leonard KJ, Dabestani RT, Paranthaman MP. Reverse Micellar Synthesis of Cerium Oxide Nanoparticles. Nanotechnology. 2005; 16:1960–1964.
19. He H-W, Wu X-Q, Ren W, Shi P, Yao X, Song Z-T. Synthesis of Crystalline Cerium Dioxide Hydrosol by a Sol-Gel Method. Ceram Int. 2012; 38(Supplement 1):S501–S504.
20. Celardo I, Pedersen JZ, Traversa E, Ghibelli L. Pharmacological Potential of Cerium Oxide Nanoparticles. Nanoscale. 2011; 3:1411–1420. [PubMed: 21369578]
21. Karakoti AS, Singh S, Kumar A, Malinska M, Kuchibhatla SVNT, Wozniak K, Self WT, Seal S. PEGylated Nanoceria as Radical Scavenger with Tunable Redox Chemistry. J Am Chem Soc. 2009; 131:14144–14145. [PubMed: 19769392]
22. Chen J, Patil S, Seal S, McGinnis JF. Rare Earth Nanoparticles Prevent Retinal Degeneration Induced by Intracellular Peroxides. Nat Nanotechnol. 2006; 1:142–150. [PubMed: 18654167]
23. Hirst SM, Karakoti A, Singh S, Self W, Tyler R, Seal S, Reilly CM. Bio-Distribution and *In Vivo* Antioxidant Effects of Cerium Oxide Nanoparticles in Mice. Environ Toxicol. 2011; 28:107–118. [PubMed: 21618676]
24. Niu J, Wang K, Kolattukudy PE. Cerium Oxide Nanoparticles Inhibit Oxidative Stress and Nuclear Factor-Kappab Activation in H9c2 Cardiomyocytes Exposed to Cigarette Smoke Extract. J Pharmacol Exp Ther. 2011; 338:53–61. [PubMed: 21464334]
25. Patil S, Kuiry SC, Seal S, Vanfleet R. Synthesis of Nanocrystalline Ceria Particles for High Temperature Oxidation Resistant Coating. J Nanopart Res. 2002; 4:433–438.
26. Zhou XD, Huebner W, Anderson HU. Processing of Nanometer-Scale CeO2 Particles. Chem Mater. 2003; 15:378–382.
27. Lee TL, Raitano JM, Rennert OM, Chan SW, Chan WY. Accessing the Genomic Effects of Naked Nanoceria in Murine Neuronal Cells. Nanomedicine. 2012; 8:599–608. [PubMed: 21889474]

28. Schubert D, Dargusch R, Raitano J, Chan SW. Cerium and Yttrium Oxide Nanoparticles are Neuroprotective. Biochem Biophys Res Commun. 2006; 342:86–91. [PubMed: 16480682]
29. Zhang H, He X, Zhang Z, Zhang P, Li Y, Ma Y, Kuang Y, Zhao Y, Chai Z. Nano-CeO2 exhibits Adverse Effects at Environmental Relevant Concentrations. Environ Sci Technol. 2011; 45:3725–3730. [PubMed: 21428445]
30. Hussain S, Al-Nsour F, Rice AB, Marshburn J, Yingling B, Ji Z, Zink JI, Walker NJ, Garantziotis S. Cerium Dioxide Nanoparticles Induce Apoptosis and Autophagy in Human Peripheral Blood Monocytes. ACS Nano. 2012; 6:5820–5829. [PubMed: 22717232]
31. Suh WH, Suslick KS, Stucky GD, Suh YH. Nanotechnology, Nanotoxicology, and Neuroscience. Prog Neurobiol. 2009; 87:133–170. [PubMed: 18926873]
32. Tseng MT, Lu X, Duan X, Hardas SS, Sultana R, Wu P, Unrine JM, Graham U, Butterfield DA, Grulke EA, et al. Alteration of Hepatic Structure and Oxidative Stress Induced by Intravenous Nanoceria. Toxicol Appl Pharmacol. 2012; 260:173–182. [PubMed: 22373796]
33. Kuchma MH, Komanski CB, Colon J, Teblum A, Masunov AE, Alvarado B, Babu S, Seal S, Summy J, Baker CH. Phosphate Ester Hydrolysis of Biologically Relevant Molecules by Cerium Oxide Nanoparticles. Nanomedicine. 2010; 6:738–744. [PubMed: 20553964]
34. Deshpande S, Patil S, Kuchibhatla SVNT, Seal S. Size Dependency Variation in Lattice Parameter and Valency States in Nanocrystalline Cerium Oxide. Appl Phys Lett. 2005; 87:133113–133116.
35. Taguchi M, Takami S, Adschiri T, Nakane T, Sato K, Naka T. Synthesis of Surface-Modified Monoclinic ZrO2 Nanoparticles Using Supercritical Water. CrystEngComm. 2012; 14:2132–2138.
36. Nel A, Xia T, Madler L, Li N. Toxic Potential of Materials at the Nanolevel. Science. 2006; 311:622–627. [PubMed: 16456071]
37. Nel AE, Madler L, Velegol D, Xia T, Hoek EM, Somasundaran P, Klaessig F, Castranova V, Thompson M. Understanding Biophysicochemical Interactions at the Nano-Bio Interface. Nat Mater. 2009; 8:543–557. [PubMed: 19525947]
38. Rogers NJ, Franklin NM, Apte SC, Batley GE, Angel BM, Lead JR, Baalousha M. Physico-Chemical Behaviour and Algal Toxicity of Nanoparticulate CeO2 In Freshwater. Environ Chem. 2010; 7:50–60.
39. Yokel RA, Florence RL, Unrine JM, Tseng MT, Graham UM, Wu P, Grulke EA, Sultana R, Hardas SS, Butterfield DA. Biodistribution and oxidative Stress Effects of a Systemically-Introduced Commercial Ceria Engineered Nanomaterial. Nanotoxicology. 2009; 3:234–248.
40. Horie M, Nishio K, Kato H, Fujita K, Endoh S, Nakamura A, Miyauchi A, Kinugasa S, Yamamoto K, Niki E, et al. Cellular Responses Induced By Cerium Oxide Nanoparticles: Induction of Intracellular Calcium Level and Oxidative Stress On Culture Cells. J Biochem. 2011; 150:461–471. [PubMed: 21693544]
41. Xia T, Kovochich M, Liong M, Madler L, Gilbert B, Shi H, Yeh JI, Zink JI, Nel AE. Comparison of the Mechanism of Toxicity of Zinc Oxide and Cerium Oxide Nanoparticles Based On Dissolution and Oxidative Stress Properties. ACS Nano. 2008; 2:2121–2134. [PubMed: 19206459]
42. Csordas G, Varnai P, Golenar T, Roy S, Purkins G, Schneider TG, Balla T, Hajnoczky G. Imaging Interorganelle Contacts and Local Calcium Dynamics at the ER-Mitochondrial Interface. Mol Cell. 2010; 39:121–132. [PubMed: 20603080]
43. Hillegass JM, Shukla A, Lathrop SA, MacPherson MB, Fukagawa NK, Mossman BT. Assessing Nanotoxicity In Cells *In Vitro* . Wiley Interdisciplinary Reviews: Nanomed Nanobiotechnol. 2010; 2:219–231.
44. Sohaebuddin S, Thevenot P, Baker D, Eaton J, Tang L. Nanomaterial Cytotoxicity Is Composition, Size, and Cell Type Dependent. Part Fibre Toxicol. 2010; 7:22. [PubMed: 20727197]
45. Lee TL, Raitano JM, Rennert OM, Chan SW, Chan WY. Accessing the Genomic Effects of Naked Nanoceria in Murine Neuronal Cells. Nanomed Nanotechnol. 2012; 8:599–608.
46. Yokel RA, Tseng MT, Dan M, Unrine JM, Graham UM, Wu P, Grulke EA. Biodistribution and Biopersistence of Ceria Engineered Nanomaterials: Size Dependence. Nanomedicine. 2012
47. Estevez AY, Pritchard S, Harper K, Aston JW, Lynch A, Lucky JJ, Ludington JS, Chatani P, Mosenthal WP, Leiter JC, et al. Neuroprotective Mechanisms of Cerium Oxide Nanoparticles in a

Mouse Hippocampal Brain Slice Model of Ischemia. Free Radic Biol Med. 2011; 51:1155–1163. [PubMed: 21704154]

48. Anderson SA, Purich DL. A Reinvestigation of Dynein Atpase Kinetics and the Inhibitory-Action of Vanadate. J Biol Chem. 1982; 257:6656–6658. [PubMed: 6211437]
49. Lark E, Omoto CK, Schumaker MF. Functional Multiplicity of Motor Molecules Revealed by a Simple Kinetic-Analysis. Biophys J. 1994; 67:1134–1140. [PubMed: 7811925]
50. Dell'Orco D, Lundqvist M, Oslakovic C, Cedervall T, Linse S. Modeling the Time Evolution of the Nanoparticle-Protein Corona in a Body Fluid. PLoS One. 2010; 5:e10949. [PubMed: 20532175]
51. Molinari M, Parker SC, Sayle DC, Islam MS. Water Adsorption and Its Effect on the Stability of Low Index Stoichiometric and Reduced Surfaces of Ceria. J Phys Chem C. 2012; 116:7073–7082.
52. Esch F, Fabris S, Zhou L, Montini T, Africh C, Fornasiero P, Comelli G, Rosei R. Electron Localization Determines Defect Formation on Ceria Substrates. Science. 2005; 309:752–755. [PubMed: 16051791]
53. Singh S, Dosani T, Karakoti AS, Kumar A, Seal S, Self WT. A Phosphate-Dependent Shift in Redox State of Cerium Oxide Nanoparticles and Its Effects on Catalytic Properties. Biomaterials. 2011; 32:6745–6753. [PubMed: 21704369]
54. Singh S, Kumar A, Karakoti A, Seal S, Self WT. Unveiling the Mechanism Of Uptake and Sub-Cellular Distribution of Cerium Oxide Nanoparticles. Mol Biosyst. 2010; 6:1813–1820. [PubMed: 20697616]
55. Das S, Singh S, Dowding JM, Oommen S, Kumar A, Sayle TX, Saraf S, Patra CR, Vlahakis NE, Sayle DC, et al. The Induction of Angiogenesis By Cerium Oxide Nanoparticles Through the Modulation of Oxygen In Intracellular Environments. Biomaterials. 2012; 33:7746–7755. [PubMed: 22858004]
56. Zhang F, Jin Q, Chan S-W. Ceria nanoparticles: Size, Size Distribution, and Shape. J Appl Phys. 2004; 95:4319–4326.
57. Cimini A, D'Angelo B, Das S, Gentile R, Benedetti E, Singh V, Monaco AM, Santucci S, Seal S. Antibody-Conjugated Pegylated Cerium Oxide Nanoparticles For Specific Targeting of a Beta Aggregates Modulate Neuronal Survival Pathways. Acta Biomater. 2012; 8:2056–2067. [PubMed: 22343002]
58. Meno SR, Nelson R, Hintze KJ, Self WT. Exposure To Monomethylarsonous Acid (MMA(III)) Leads To Altered Selenoprotein Synthesis in a Primary Human Lung Cell Model. Toxicol Appl Pharmacol. 2009; 239:130–136. [PubMed: 19095002]
59. Nandy B, Joshi A, Ali ZS, Sen S, Prasad NG. Degree of Adaptive Male Mate Choice Is Positively Correlated With Female Quality Variance. Sci Rep. 2012; 2:447. [PubMed: 22685628]
60. Trogadas P, Parrondo J, Ramani V. CeO(2) Surface Oxygen Vacancy Concentration Governs *In Situ* Free Radical Scavenging Efficacy in Polymer Electrolytes. ACS Appl Mater Interfaces. 2012; 4:5098–6102. [PubMed: 22999007]
61. Weber WH, Hass KC, McBride JR. Raman, study of CeO2: Second-order Scattering, Lattice Dynamics, and Particle-Size Effects. Phys Rev B Condens Matter. 1993; 48:178–185. [PubMed: 10006765]
62. Feng XD, Sayle DC, Wang ZL, Paras MS, Santora B, Sutorik AC, Sayle TXT, Yang Y, Ding Y, Wang XD, et al. Converting Ceria Polyhedral Nanoparticles Into Single-Crystal Nanospheres. Science. 2006; 312:1504–1508. [PubMed: 16763144]
63. Sayle TXT, Cantoni M, Bhatta UM, Parker SC, Hall SR, Mobus G, Molinari M, Reid D, Seal S, Sayle DC. Strain and Architecture-Tuned Reactivity in Ceria Nanostructures; Enhanced Catalytic Oxidation of CO to CO2. Chem Mater. 2012; 24:1811–1821.

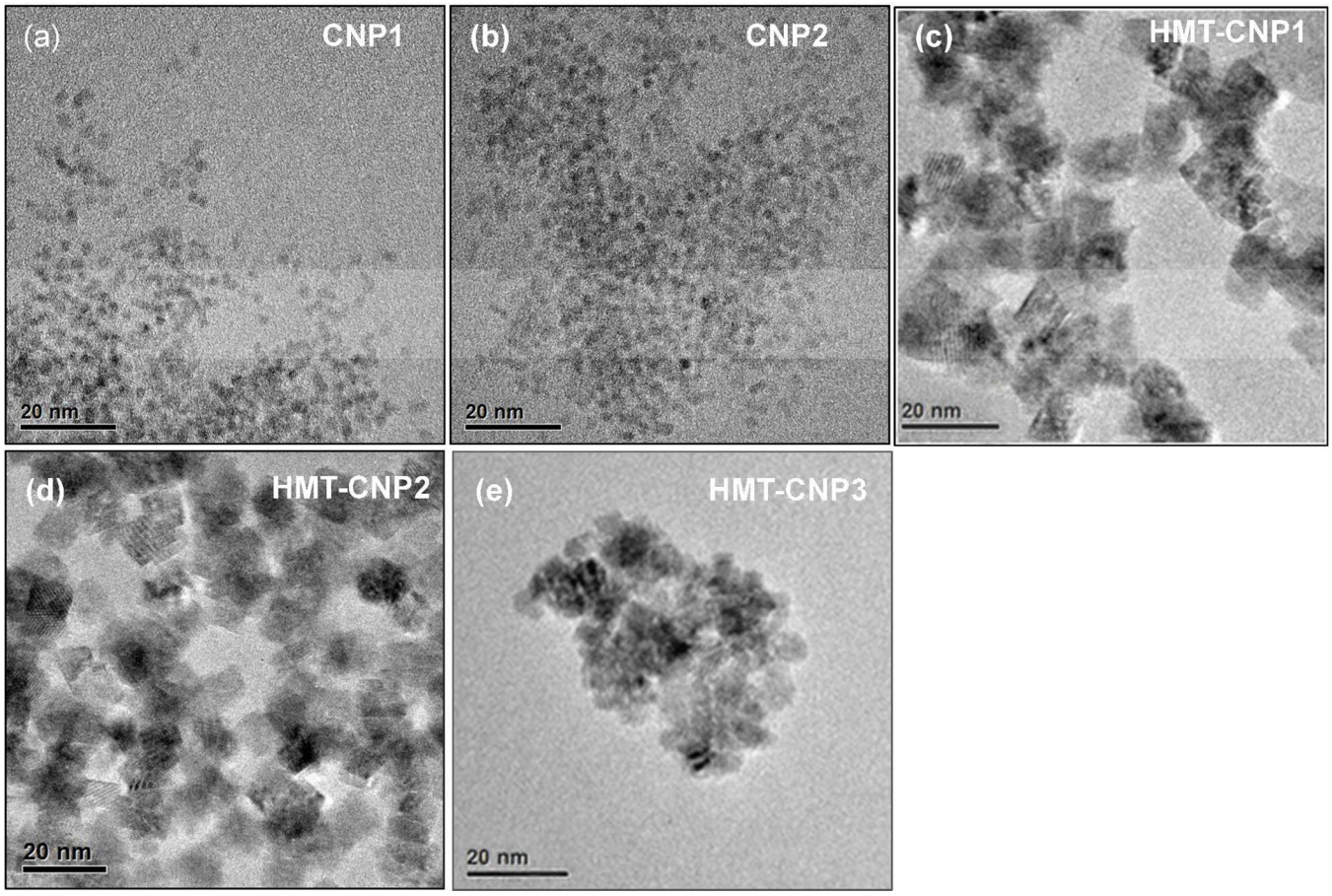

Figure 1.

Size, shape, and morphology variation of Cerium Oxide Nanoparticles (CeO_2) NPs synthesized by two different synthesis methods. TEM images of CeO_2 NPs prepared using water-based (a & b) or solvent HMT (c – e) synthesis methods. (a) CNP1. (b) CNP2. (c) HMT-CNP1. (d) HMT-CNP2. (e) HMT-CNP3.

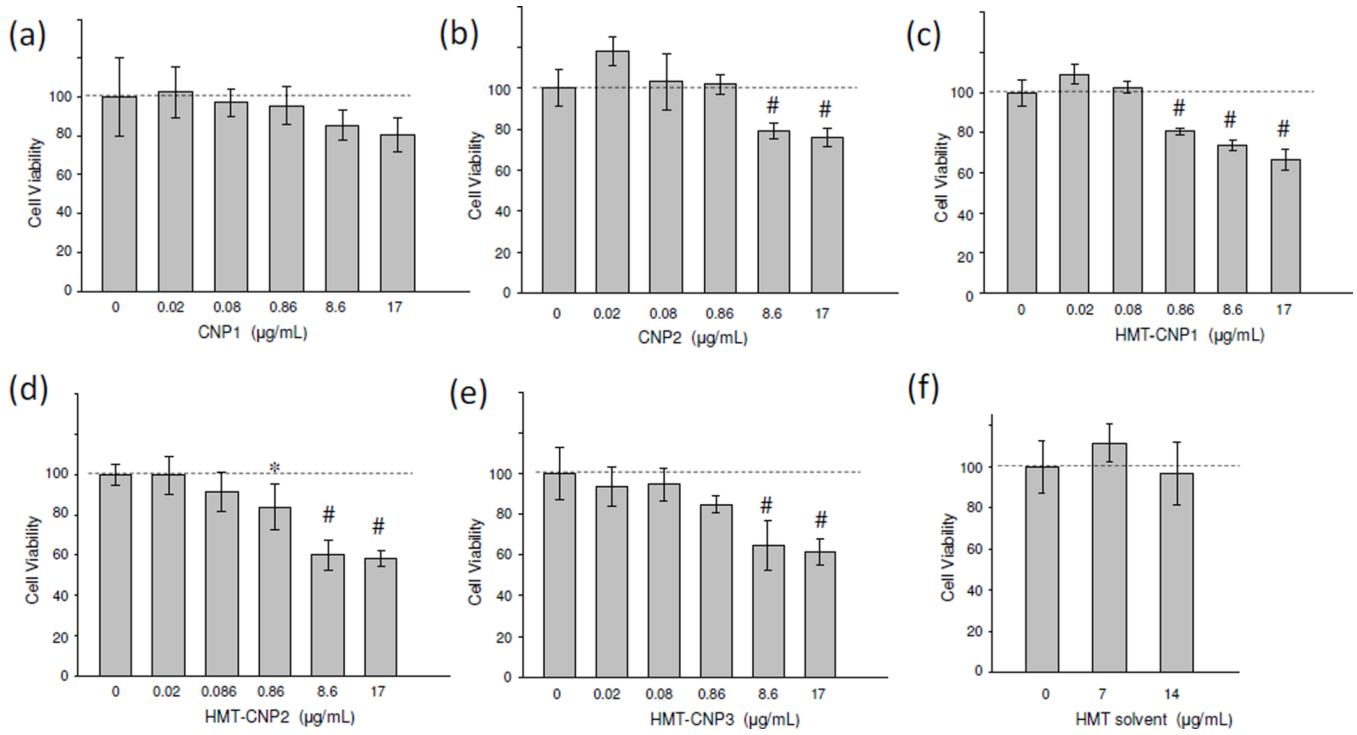

Figure 2.

Cell viability of HUVECs exposed to various preparations of CeO_2 NPs. HUVEC cells were exposed to increasing CeO_2 NPs concentrations (0, 0.02, 0.08, 0.86, 8.6, 17 μg/mL). (a) CNP1. (b) CNP2. (c) HMT-CNP1. (d) HMT-CNP2. (e) HMT-CNP3. Cell viability was determined by dividing the absorbance of treated samples to untreated controls and reported as a percentage of control cells. The mean of at least 4 independent cultures is plotted with standard deviation as error. #, $p \leq 0.001$.

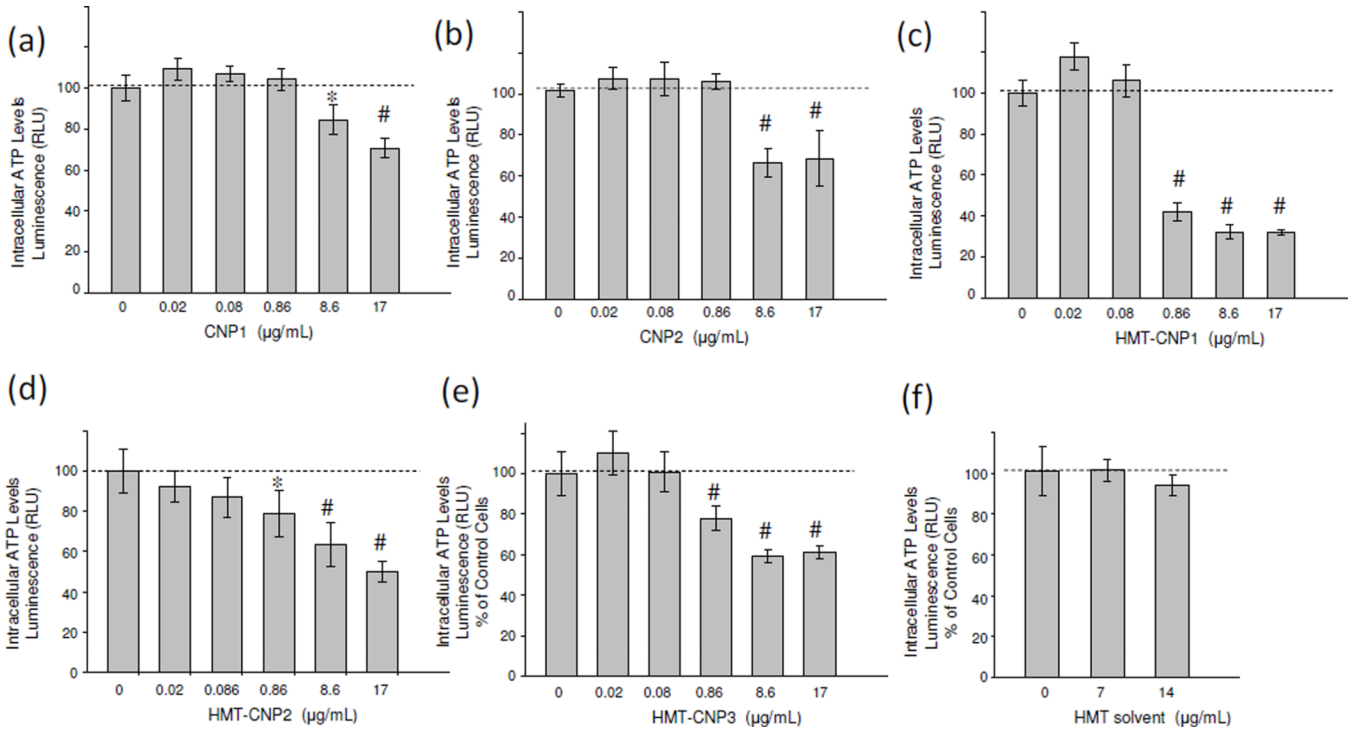

Figure 3.

Intercellular ATP levels of HUVECs exposed to various preparations of CeO_2 NPs. HUVEC cells were exposed to increasing CeO_2 NP concentrations (0.02, 0.08, 0.86, 8.6 17 μg/mL). (a) CNP1. (b) CNP2. (c) HMT-CNP1. (d) HMT-CNP2. (e) HMT-CNP3. ATP level was determined by dividing the luminescence of treated samples to untreated controls and reported as a percentage of control cells. The mean of at least 4 independent cultures is plotted with standard deviation as error. *, $p \leq 0.05$, #, $p \leq 0.001$.

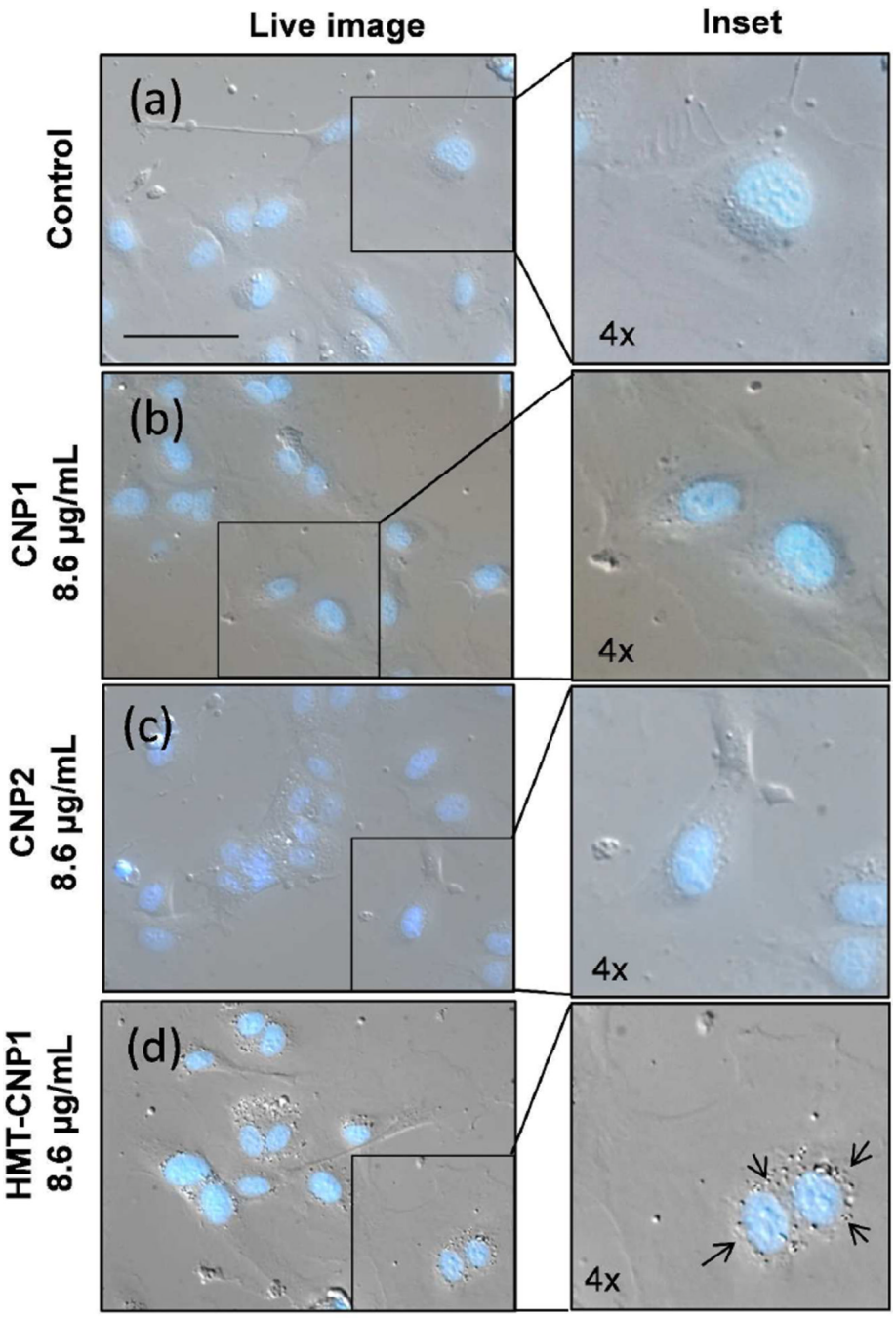

Figure 4.

Live cell examination of HUVEC cells exposed to HMT-CNP1. HUVEC cells were exposed to 8.6 µg/mL CeO_2 NPs for 20 h. (a) Control cells. (b) CNP1. (c) CNP2. (d) HMT-CNP1. Hoescht dye was added just before imaging to show location of nuclei. Representative images feature 4x zoom of region of interest. Scale bar = 50 µm.

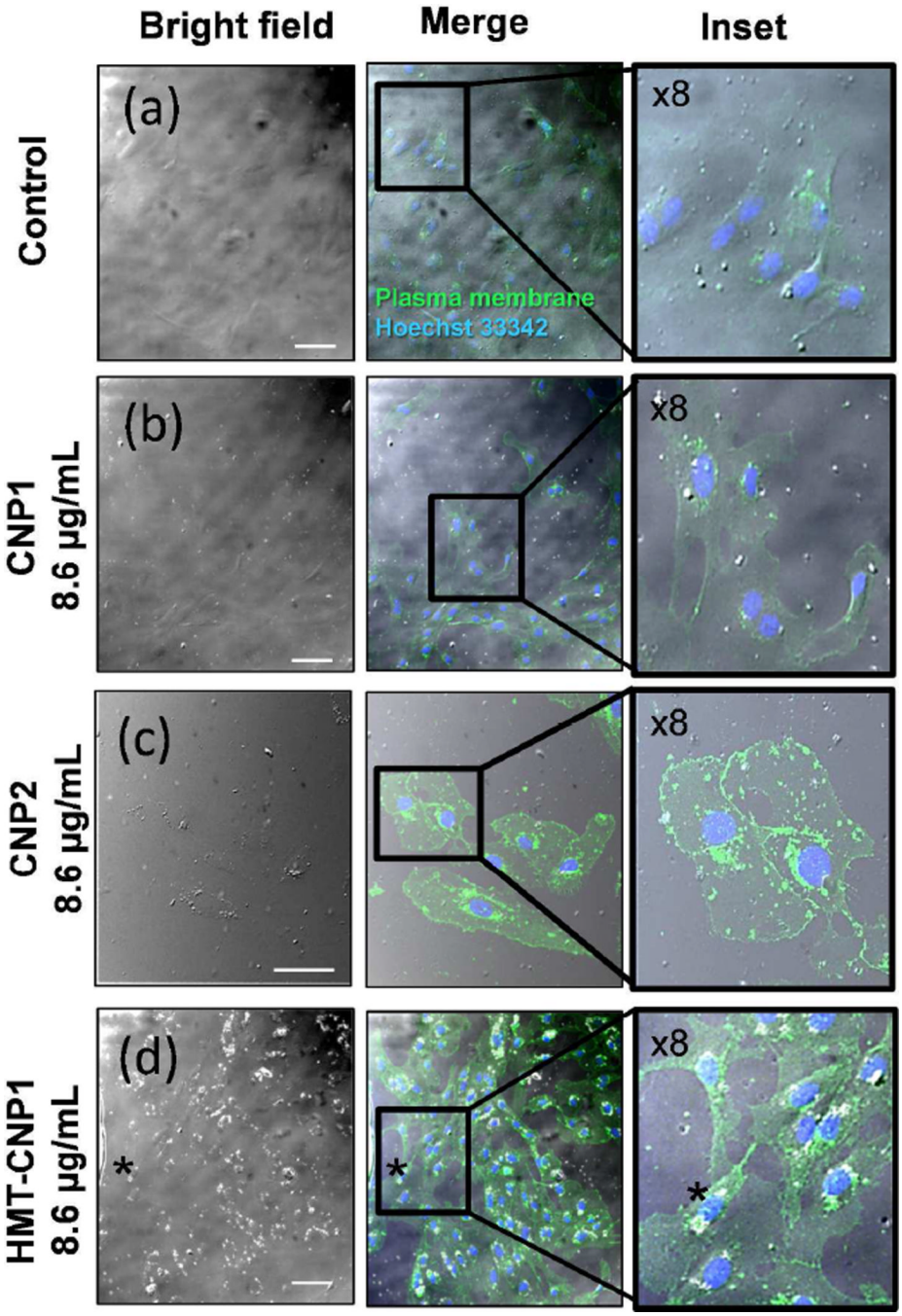

Figure 5.

Intracellular aggregation of HMT-CNP1 as viewed by confocal laser scanning microscopy (CLSM). Cells were exposed to nanoparticles for 24 h, washed, trypsinized and seeded onto glass coverslips for 4 h (to allow for attachment), fixed and labeled with antibody for identification of plasma membranes (green channel) and Hoechst 33342 (blue channel) for identification of nuclei. (a) Control/no treatment (b) 8.6 µg/mL CNP1 (c) 8.6 µg/mL CNP2 (d) 8.6 µg/mL HMT-CNP1. Scale bar = 50 µM. Asterisk follows representative region of HMT-CNP1 aggregation.

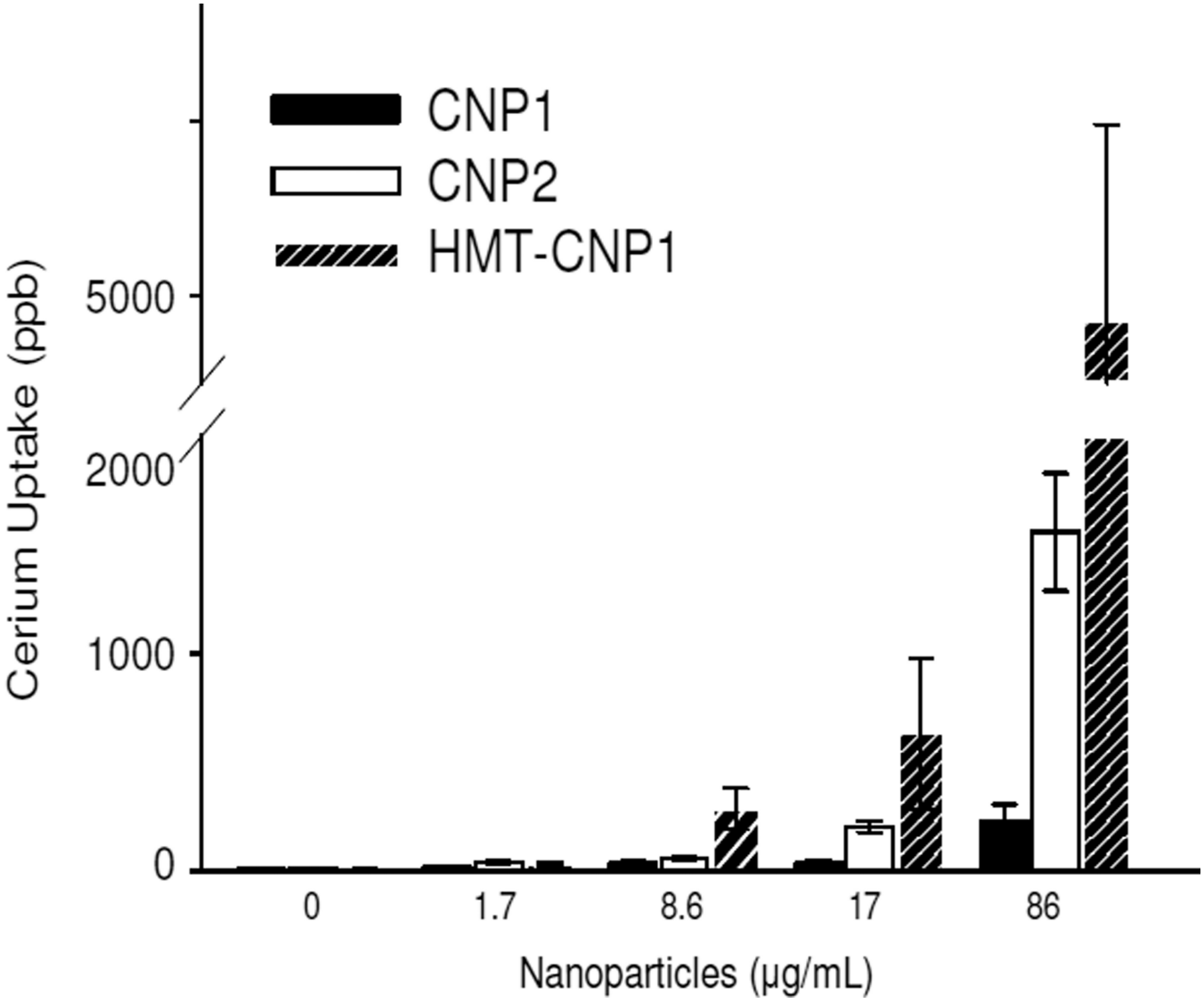

Figure 6.

Increased uptake of HMT-CNP1 as measured by ICP-MS. HUVEC cells were incubated with various CeO_2 NPs for 24 h, washed two-times to remove extracellular nanoparticles, collected by typsination and washed with PBS again to remove excess media and particles which may be adsorbed on the surface of the cells. The concentration of cerium inside cells was measured by ICP-MS as described in methods.

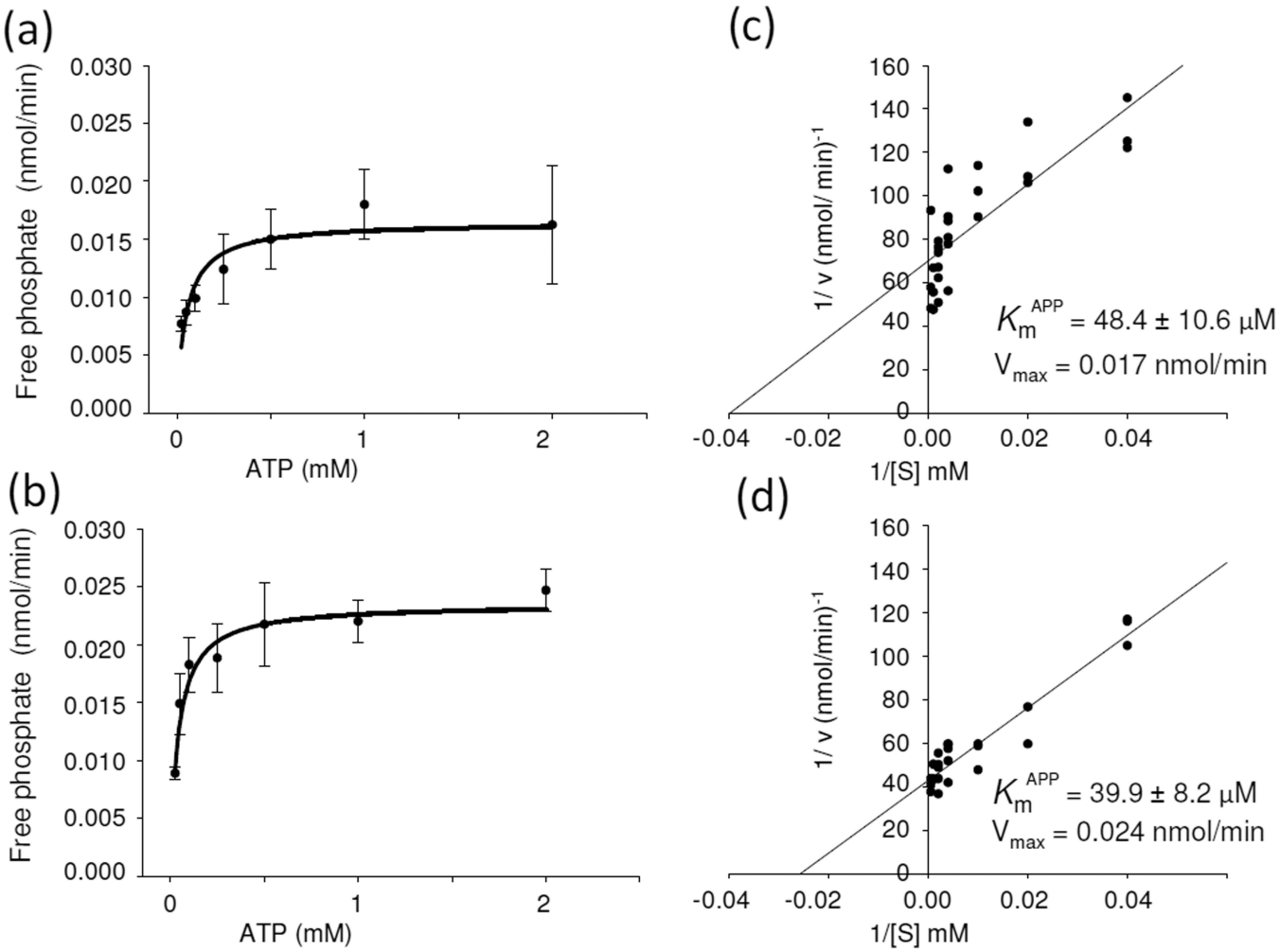

Figure 7.

CNP2 and HMT-CNP1s exhibit significant ATPase activity at physiologically relevant concentrations of ATP. ATPase activity of CeO_2 NPs was quantified by measuring phosphate released with EnzCheck® phosphate assay using varying concentrations of ATP with 34 μg/mL NPs. (a) CNP2. (b) HMT-CNP1. Line plot is representative of 3 or more experiments. Double reciprocal plots of ATPase activity with ATP as substrate using constant concentration of NPs (34 μg/mL). (c) CNP2. (d) HMT-CNP1.

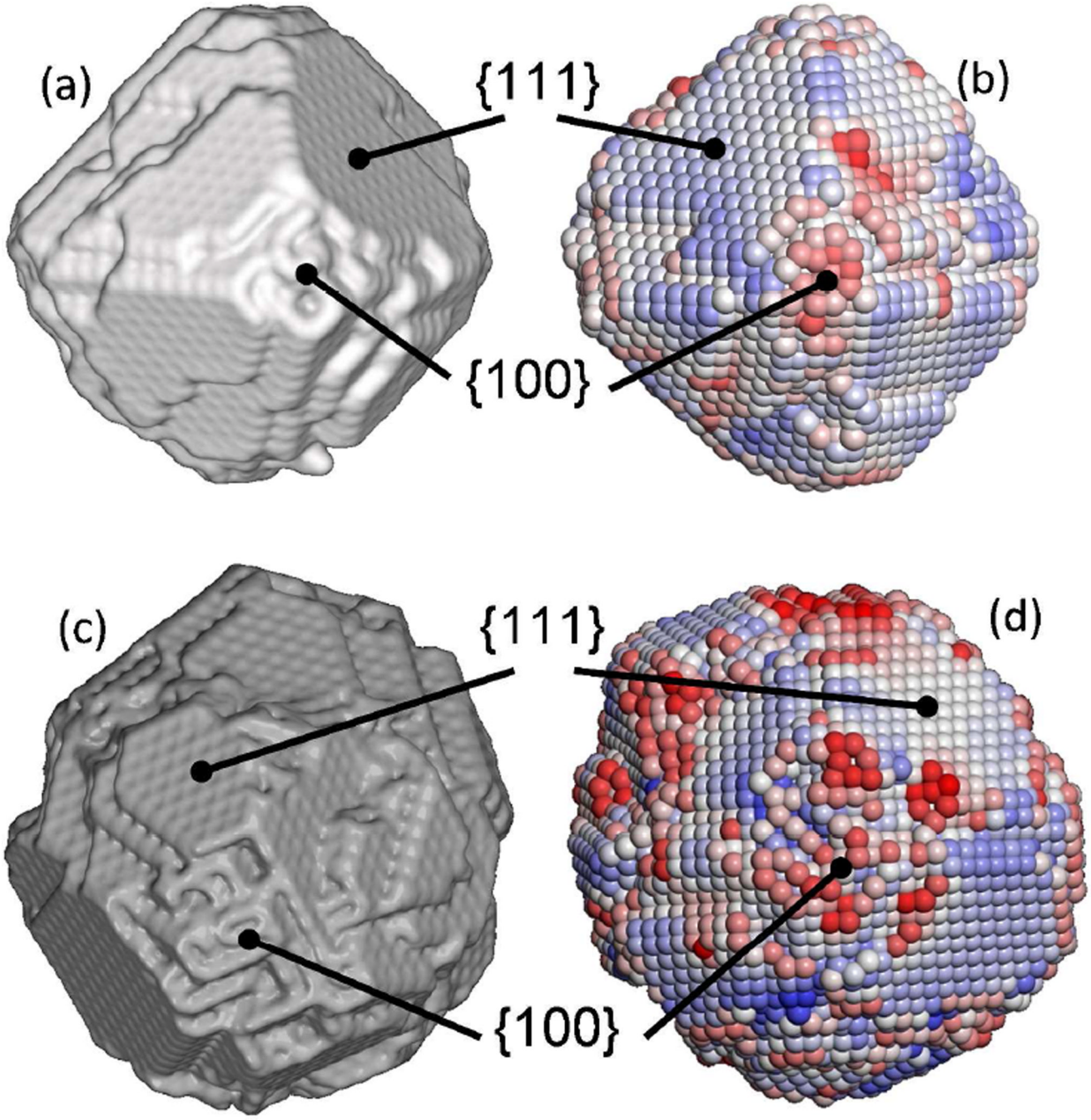

Figure 8.
Atomistic models of ceria nanoparticles (CNP). (a) Surface rendered model of a CNP with polyhedral morphology; (b) reactivity fingerprint of the polyhedral CNP; (c) surface rendered model of a CNP with 'spherical' morphology; (d) reactivity fingerprint of the spherical CNP.

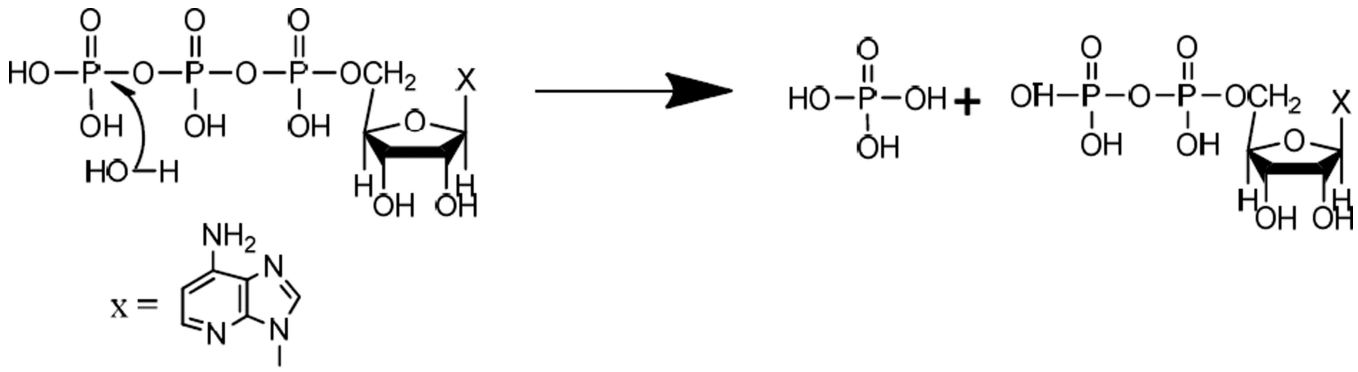

Scheme 1.

Table 1

Physico-chemical properties of cerium oxide nanoparticles (CeO_2) prepared by water-based or HMT-based method.

Particle Characteristics	**CNP1**	**CNP2**	**HMT-CNP1**	**HMT-CNP2**	**HMT-CNP3**
Morphology	round	round	polygonal	polygonal	round
Crystalline property	crystalline fluorite structure	crystalline fluorite structure	crystalline fluorite structure	crystalline fluorite structure	crystalline fluorite structure
Size (TEM) (nm)	3–5	5–8	10–15	10–15	8–10
Hydrodynamic radii (nm)	30.84 ±2.8	69.26 ±4.5	147.70 ±6.4	83.56 ±3.2	129.20 ±4.1
Zeta potential (mV)	18.6 ±0.6	30.2 ±1.5	34.6 ±1.7	38.6 ±2.3	36.7 ±2.1
Hexamethyltetramine (% wt)	-	-	1.68 ±0.2	8.16 ±0.7	1.78±0.3
Surface Ce^{3+}/Ce^{4+} ratio	1.28	0.37	0.37	0.36	0.32
BET (m^2/g)	92	102	86	71	118

Table 2

Synthesis method determines surface character and catalytic activities of CeO_2 NPs. Various properties of CeO_2 NPs have been tested for their ability to exhibit SOD mimetic[6], catalase mimetic[7], ·NO scavenging[4] , phosphatase or ATPase activities.

Catalytic activity	**Assay**	**CNP1**	**CNP2**	**HMT-CNP1**	**SiO_2**
Phosphatase	pNPP	no	yes	yes	no
ATPase	Malachite Green	no	yes	yes	no
	ENZCheck	no	yes	yes	n/d
•NO Scavenger	CuFl assay	no [4]	yes [4]	no	no [4]
Catalase Mimetic	UV-visible	no [7]	yes [7]	no	no
SOD Mimetic	Cytochrome C	yes [6]	no [6]	no	no

n/d = not determined